Inorg. Chem. **2004**, *43*, 4645–4662

The Coordination Chemistry of "[BP_3]NiX" Platforms: Targeting Low-Valent Nickel Sources as Promising Candidates to $L_3Ni{=}E$ and $L_3Ni{\equiv}E$ Linkages

Cora E. MacBeth, J. Christopher Thomas, Theodore A. Betley, and Jonas C. Peters*

Division of Chemistry and Chemical Engineering, Arnold and Mabel Beckman Laboratories of Chemical Synthesis, California Institute of Technology, Pasadena, California 91125

Received January 15, 2004

A series of divalent, monovalent, and zerovalent nickel complexes supported by the electron-releasing, monoanionic tris(phosphino)borate ligands [$PhBP_3$] and [$PhBP^{iPr}_3$] ([$PhBP_3$] = [$PhB(CH_2PPh_2)_3]^-$, [$PhBP^{iPr}_3$] = [$PhB(CH_2P^iPr_2)_3]^-$) have been synthesized to explore fundamental aspects of their coordination chemistry. The pseudotetrahedral, divalent halide complexes [$PhBP_3$]NiCl (**1**), [$PhBP_3$]NiI (**2**), and [$PhBP^{iPr}_3$]NiCl (**3**) were prepared by the metalation of [$PhBP_3$]Tl or [$PhBP^{iPr}_3$]Tl with $(Ph_3P)_2NiCl_2$, NiI_2, and $(DME)NiCl_2$ (DME = 1,2-dimethoxyethane), respectively. Complex **1** is a versatile precursor to a series of complexes accessible via substitution reactions including [$PhBP_3$]-Ni(N_3) (**4**), [$PhBP_3$]Ni($OSiPh_3$) (**5**), [$PhBP_3$]Ni(O-*p*-^{t}Bu-Ph) (**6**), and [$PhBP_3$]Ni(S-*p*-^{t}Bu-Ph) (**7**). Complexes **2**–**5** and **7** have been characterized by X-ray diffraction (XRD) and are pseudotetrahedral monomers in the solid state. Complex **1** reacts readily with oxygen to form the four-electron-oxidation product, {[$PhB(CH_2P(O)Ph_2)_2(CH_2PPh_2)$]-NiCl} (**8A** or **8B**), which features a solid-state structure that is dependent on its method of crystallization. Chemical reduction of **1** using Na/Hg or other potential 1-electron reductants generates a product that arises from partial ligand degradation, [$PhBP_3$]Ni(η^2-CH_2PPh_2) (**9**). The more sterically hindered chloride **3** reacts with Li(dbabh) (Hdbabh = 2,3:5,6-dibenzo-7-azabicyclo[2.2.1]hepta-2,5-diene) to provide the three-coordinate complex [κ^2-$PhBP^{iPr}_3$]Ni(dbabh) (**11**), also characterized by XRD. Chemical reduction of complex **1** in the presence of L-type donors produces the tetrahedral Ni(I) complexes [$PhBP_3$]Ni(PPh_3) (**12**) and [$PhBP_3$]Ni(CN^tBu) (**13**). Reduction of **3** following the addition of PMe_3 or *tert*-butyl isocyanide affords the Ni(I) complexes [$PhBP^{iPr}_3$]Ni(PMe_3) (**14**) and [$PhBP^{iPr}_3$]Ni(CN^tBu) (**15**), respectively. The reactivity of these [$PhBP_3$]Ni^{I}L and [$PhBP^{iPr}_3$]Ni^{I}L complexes with respect to oxidative group transfer reactions from organic azides and diazoalkanes is discussed. The zerovalent nitrosyl complex [$PhBP_3$]Ni(NO) (**16**) is prepared by the reaction of **1** with excess NO or by treating **12** with stoichiometric NO. The anionic Ni(0) complexes [[κ^2-$PhBP_3$]Ni$(CO)_2$][^{n}Bu_4N] (**17**) and [[κ^2-$PhBP^{iPr}_3$]Ni$(CO)_2$][ASN] (**18**) (ASN = 5-azoniaspiro[4.4]nonane) have been prepared by reacting [$PhBP_3$]Tl or [$PhBP^{iPr}_3$]Tl with $(Ph_3P)_2Ni(CO)_2$ in the presence of R_4NBr. The photolysis of **17** appears to generate a new species consistent with a zerovalent monocarbonyl complex which we tentatively assign as {[$PhBP_3$]Ni(CO)}{^{n}Bu_4N}, although complete characterization of this complex has been difficult. Finally, theoretical DFT calculations are presented for the hypothetical low spin complexes [$PhBP_3$]Ni(N^tBu), [$PhBP^{iPr}_3$]Ni(N^tBu), [$PhBP^{iPr}_3$]Ni(NMe), and [$PhBP^{iPr}_3$]Ni(N) to consider what role electronic structure factors might play with respect to the relative stability of these species.

I. Introduction

The fundamental coordination chemistry of mid-to-late first row transition metal ions supported by relatively simple ligand auxiliaries represents a mature field that has experienced somewhat of a renaissance in recent years. Much of the renewed interest has been sparked by the realization that these types of species can participate in a host of catalytic group transfer reactions such as aziridinations,[1] cyclopropanations,[2] and oxidations.[3] Moreover, there is hope that new approaches to catalytic small molecule activation and functionalization reactions that exploit reactive metal fragments from this sector of the transition block may yet be elucidated.[4,5] Small molecule substrates of interest might include

* Author to whom correspondence should be addressed. E-mail: jpeters@caltech.edu.

10.1021/ic049936p CCC: $27.50
Published on Web 06/25/2004

N_2, N_2O, O_2, CO_2, CO, and P_4.[6] One of the most attractive features of the mid-to-late first row ions concerns their ability to form metal-to-ligand multiple bond linkages that are kinetically and thermodynamically reactive. Species of these types (e.g., M═O, M═CR_2, M═NR, M≡N) are proposed as key intermediates in a number of catalytic reactions of both synthetic and biocatalytic significance.[3,7]

Very recently, several groups have reported the isolation of well-defined later first row complexes that feature metal-to-ligand multiple bond linkages. For example, using sterically encumbering bis(phosphine) ligands, Hillhouse and co-workers have shown that L_2Ni fragments are compatible with imide (NR),[8] phosphinidene (PR),[9] and carbene (CR_2)[10] functional groups (generally defined as L_2Ni^{II}═E species). These fascinating complexes, which follow on an early observation from the Jones group that provided strong evidence for a reactive L_2Ni^{II}═S linkage,[11] have since been shown to undergo stoichiometric group transfer processes, for instance to ethylene.[12,13] The L_2Ni^{II}═E systems owe their appreciable stability to a combination of simple electronic factors and to the considerable steric protection provided by the bulky bis(phosphine) ligand and the substitution pattern at the multiply bonded functional group. Four-coordinate pseudotetrahedral systems that feature M═E and M≡E linkages (i.e., L_3M≡E systems) are equally intriguing targets, and a more general understanding of the electronic similarities and differences that dictate the relative stability of later first row metal M═E and M≡E linkages for three-, four-, and higher coordinate structures is clearly of interest. In this context, our group has initiated the development of pseudotetrahedral "L_3MX" platforms where L_3 represents the anionic tris(phosphine) donor [$PhBP_3$] or [$PhBP^{iPr}_3$] ([$PhBP_3$] = $[PhB(CH_2PPh_2)_3]^-$, [$PhBP^{iPr}_3$] = $[PhB(CH_2P^iPr_2)_3]^-$) and M represents a first row ion such as Fe or Co, and in this paper Ni.[14−18] Our interest in the family of nickel complexes described herein is motivated by recent findings demonstrating that "L_3Co" and "L_3Fe" complexes supported by BP_3 ligand auxiliaries (i) support later metal-to-ligand triple bond linkages (e.g., L_3Co≡NR, L_3Fe≡NR, L_3Fe≡N) and (ii) participate in multielectron group transfer reactions that accept and release the multiply bonded functional unit. Riordan's group has moreover shown that "$L_3Ni(I)$" species supported by anionic tris(thioether)borate ligands undergo oxidative group transfer with dioxygen. For example, the Ni(I) carbonyl supported by [$PhTt^{tBu}$] reacts with dioxygen to form a $Ni_2(\mu\text{-}O)_2$ structure in which each nickel center has been oxidized to Ni(III).[19] This structure type was first elucidated for nickel by Hikichi and co-workers using a tris(pyrazolyl)borate auxiliary scaffold.[20]

The present report focuses on the synthesis and characterization of a host of nickel complexes supported by BP_3 ligands and on theoretical and reactivity issues pertinent to the possible construction of L_3Ni═E and L_3Ni≡E linkages. To these ends, we have prepared a series of divalent L_3NiX (X = I, Cl, N_3, OR, or SR) complexes, as well as mono- and zerovalent nickel precursors. Where applicable, structural and electronic comparisons are made between these "[$PhBP_3$]Ni" and "[$PhBP^{iPr}_3$]Ni" systems and their structurally similar counterparts supported by other anionic and facially capping ligand auxiliaries,[21,22] or by neutral tris(phosphine) ligand auxiliaries such as $CH_3C(CH_2PPh_2)_3$ and $PhP(CH_2PPh_2)_2$.[23,24] The results presented demonstrate that tris(phosphino)borate scaffolds effectively stabilize the lower oxidation states of nickel (e.g., Ni^0, Ni^I, and Ni^{II}) while in most cases maintaining a four-coordinate pseudotetrahedral geometry. Synthetic

(1) (a) Evans, D. A.; Woerpol, K. A.; Hinman, M. M.; Faul, M. M. *J. Am. Chem. Soc.* **1991**, *113*, 726−728. (b) Li, Z.; Quan, R. W.; Jacobsen, E. N. *J. Am. Chem. Soc.* **1995**, *117*, 5889−5890. (c) Muller, P.; Fruit, C. *Chem. Rev.* **2003**, *103*, 2905−2919. (d) Jacobson, E. N. In *Comprehensive Asymmetric Catalysis;* Jacobsen, E. N., Pfaltz, A., Yamamoto, H., Eds.; Springer: Hamburg, 1999.

(2) (a) Doyle, M. P.; McKervey, M. A.; Ye, T. *Modern Catalytic Methods for Organic Synthesis with Diazo Compounds*; Wiley: New York, 1998. (b) Brookhart, M.; Studabaker, W. B. *Chem. Rev.* **1987**, *87*, 411−432. (c) Doyle, M. P. *Chem. Rev.* **1986**, *86*, 919−939.

(3) Collman, J. P.; Hegedus, L. S.; Norton, J. R.; Finke, R. G. *Principles and Applications of Organotransition Metal Chemistry*, 2nd ed.; University Science Books: Mill Valley, CA, 1987.

(4) Fisher, B.; Eisenberg, R. *J. Am. Chem. Soc.* **1980**, *102*, 7361−7363.

(5) Morgenstern, D. A.; Wittrig, R. E.; Fanwick, P. E.; Kubiak, C. P. *J. Am. Chem. Soc.* **1993**, *115*, 6470−6471.

(6) For examples, see: (a) Detrich, J. L.; Konečný, R.; Vetter, W. M.; Doren, D.; Rheingold, A. L.; Theopold, K. H. *J. Am. Chem. Soc.* **1996**, *118*, 1703−1712. (b) Cecconi, F.; Ghilardi, C. A.; Midollini, S.; Moneti, S.; Orlandini, A.; Bacci, M. *J. Chem. Soc., Chem. Commun.* **1985**, 731−733. (c) Ehses, M.; Romerosa, A.; Peruzzi, M. *Top. Curr. Chem.* **2002**, *220*, 107−140. (d) Matsunaga, P. T.; Hillhouse, G. L.; Rheingold, A. L. *J. Am. Chem. Soc.* **1993**, *115*, 2075−2077. (e) Qin, Z.; Thomas, C. M.; Lee, S.; Coates, G. W. *Angew. Chem., Int. Ed.* **2003**, *42*, 5484−5487. (f) Fox, D. J.; Bergman, R. G. *J. Am. Chem. Soc.* **2003**, *125*, 8984−8985. (g) Holland, P. L.; Andersen, R. A.; Bergman, R. G. *J. Am. Chem. Soc.* **1996**, *118*, 1092−1104.

(7) *Bioinorganic Catalysis;* Reedijk, J., Bouwman, E., Eds.; Marcel Dekker: New York, 1999.

(8) Mindiola, D. J.; Hillhouse, G. L. *J. Am. Chem. Soc.* **2001**, *123*, 4623−4624.

(9) Melenkivitz, R.; Mindiola, D. J.; Hillhouse, G. L. *J. Am. Chem. Soc.* **2002**, *124*, 3846−3847.

(10) Mindiola, D. J.; Hillhouse, G. L. *J. Am. Chem. Soc.* **2002**, *124*, 9976−9977.

(11) Vicic, D. A.; Jones, W. D. *J. Am. Chem. Soc.* **1999**, *121*, 4070−4071.

(12) Waterman, R.; Hillhouse, G. L. *J. Am. Chem. Soc.* **2003**, *125*, 13350−13351.

(13) Waterman, R.; Hillhouse, G. L. *Organometallics* **2003**, *22*, 5182−5184.

(14) Jenkins, D. M.; Betley, T. A.; Peters, J. C. *J. Am. Chem. Soc.* **2002**, *124*, 11238−11239.

(15) Brown, S. D.; Betley, T. A.; Peters, J. C. *J. Am. Chem. Soc.* **2003**, *125*, 322−323.

(16) Betley, T. A.; Peters, J. C. *J. Am. Chem. Soc.* **2003**, *125*, 10782−10783.

(17) Brown, S. D.; Peters, J. C. *J. Am. Chem. Soc.* **2004**, *126*, 4538−4539.

(18) Betley, T. A.; Peters, J. C. *J. Am. Chem. Soc.* **2004**, *126*, 6252−6254.

(19) Mandimutsira, B. S.; Yamarik, J. L.; Brunold, T. C.; Weiwei, G.; Cramer, S. P.; Riordan, C. G. *J. Am. Chem. Soc.* **2001**, *123*, 9194−9195.

(20) Hikichi, S.; Yoshizawa, M.; Sasakura, Y.; Akita, M.; Moro-Oka, Y. *J. Am. Chem. Soc.* **1998**, *120*, 10567−10568.

(21) Kubiak and coworkers have examined related [$PhBP_3$]Ni systems: Kubiak, C. P. et al. Private communication, 2004.

(22) For examples of Ni complexes supported by [Tp] ligands see: (a) Gutierrez, E.; Hudson, S. A.; Monge, A.; Nicasio, M. C.; Paneque, M. *J. Organomet. Chem.* **1998**, *551*, 215−227. (b) Shirasawa, N.; Nguyet, T. T.; Hikichi, S.; Moro-oka, Y.; Akita, M. *Organometallics* **2001**, *20*, 3582−3598. (c) Uehara, K.; Hikichi, S.; Akita, M.; Muneta, A. *J. Chem. Soc., Dalton Trans.* **2002**, 3529−3538. (d) Trofimenko, S. *Scorpionates−The Coordination Chemistry of Polypyrazolylborate Ligands;* Imperial College Press: London, 1999.

(23) Dapporto, P.; Fallani, G.; Sacconi, L. *Inorg. Chem.* **1974**, *13*, 2847−2850.

(24) (a) Hou, H.; Gantzel, P. K.; Kubiak, C. P. *Organometallics* **2003**, *22*, 2817−2819. (b) Hou, H.; Gantzel, P. K.; Kubiak, C. P. *J. Am. Chem. Soc.* **2003**, *125*, 9564−9565.

Scheme 1

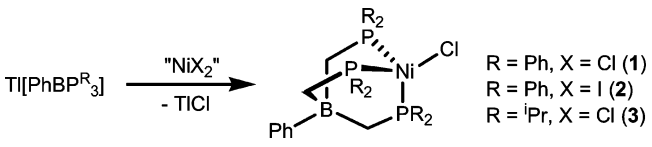

access to $L_3Ni^{III}{\equiv}E$ and $L_3Ni^{IV}{\equiv}E$ species remains a synthetic challenge.

II. Results and Discussion

IIa. Synthesis and Characterization of Pseudotetrahedral [PhBP$_3$]Ni^{II}X and [PhBP$^{iPr}_3$]Ni^{II}X Complexes. Of interest as synthetic precursors to the nickel chemistry featured herein are the Ni(II) halides [PhBP$_3$]NiX and [PhBP$^{iPr}_3$]NiX, where X = Cl or I. Divalent complexes of these types have already been reported for [PhBP$_3$]- and [PhBP$^{iPr}_3$]-supported iron and cobalt systems,[25] and a synthetic protocol that exploits [PhBP$_3$]Tl or [PhBP$^{iPr}_3$]Tl as a transmetalation reagent is equally effective for nickel. Thus, [PhBP$_3$]Tl reacts with the nickel precursors $(Ph_3P)_2NiCl_2$ or NiI_2 to eliminate TlX (X = Cl, I) and generate the desired green [PhBP$_3$]NiCl (**1**) and red-brown [PhBP$_3$]NiI (**2**) halide complexes (Scheme 1) in good yield. $NiCl_2$ could also be used as a starting material, affording some **1** upon reaction with [PhBP$_3$]Tl, but undesirable side reactions proved more problematic. Similarly, the synthesis of the yellow-green $S = 1$ complex [PhBP$^{iPr}_3$]NiCl (**3**) is achieved in high isolated yield (>90%) by reaction of the starting material (DME)-$NiCl_2$ (DME = 1,2-dimethoxyethane) with [PhBP$^{iPr}_3$]Tl. Evans method measurements of **1**, **2**, and **3** in benzene solution are consistent with two unpaired electrons per nickel center. The attempted synthesis of **3** using other Ni(II) precursors, such as $(Ph_3P)_2NiCl_2$ and $NiCl_2$, again provides some **3**; however, the desired product is accompanied by large amounts of diamagnetic impurities in each case. These types of electron-transfer reactions would generate a reactive borane radical that then would be expected to undergo bond homolysis to liberate a $^{\bullet}CH_2PR_2$ radical. The [PhBP$^{iPr}_3$] anion is inherently more reducing than its [PhBP$_3$] counterpart, and, as a result, its installation at nickel is somewhat more sensitive.

The solid-state structures of **2** and **3** were determined by X-ray diffraction (XRD) studies on single crystals of **2** and **3** (Figure 1). Each of the halide complexes is four-coordinate and pseudotetrahedral, and the bond lengths and angles are for the most part unremarkable. The iodide complex **2** features two short (2.265(2) and 2.267(2) Å) and one modestly longer Ni−P (2.289(2) Å) bond, whereas the chloride complex **3** exhibits three nearly equidistant bond lengths (2.2871(8), 2.2893(9), and 2.2811(8) Å). The P−Ni−P angles are on average slightly larger for **3** (94−95°) than for **2** (91.5−94°). One comparison worth noting is that the Ni−I bond length in **2** is appreciably longer (2.498(1) Å) than the Ni−I bond length in the isostructural but cationic

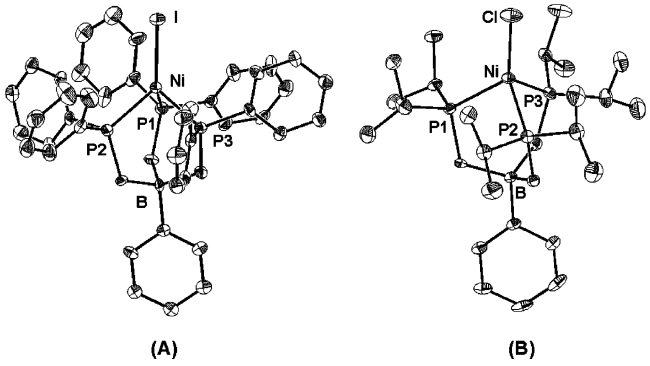

Figure 1. Displacement ellipsoid representations (50%) of (A) [PhBP$_3$]-NiI (**2**) and (B) [PhBP^{i}Pr$_3$]NiCl (**3**). Hydrogen atoms and solvent molecules have been omitted for clarity. Selected interatomic distances (Å) and angles (deg) for **2**: Ni−I, 2.498(1); Ni−P1, 2.289(2); Ni−P2, 2.265(2); Ni−P3, 2.267(2); Ni−B, 3.484(6); P1−Ni−P3, 91.52(6); P1−Ni−P2, 93.77(6); P2−Ni−P3, 92.99(6); I−Ni−P1, 124.25(5); I−Ni−P2, 118.33(6); I−Ni−P3, 127.20(5). For **3**: Ni−Cl, 2.1772(9); Ni−P1, 2.2871(8); Ni−P2, 2.2893(9); Ni−P3, 2.2811(8); Ni−B, 3.474(3); P1−Ni−P2, 94.12(3); P2−Ni−P3, 94.97(3); P1−Ni−P3, 94.16(3); Cl−Ni−P1, 125.30(4); Cl−Ni−P2, 121.92(4); Cl−Ni−P3, 118.94(3).

Scheme 2

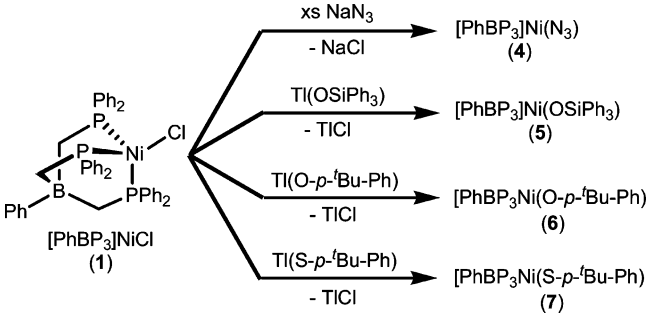

$[L_3NiI]^+$ species $[(CH_3C(CH_2PPh_2)_3)NiI][As_6I_8]$ (2.414(4) Å).[26] Hence, placing a formal positive charge on the $[L_3NiI]^+$ fragment attracts the iodide anion closer to the nickel center. While **2** can be formally described as zwitterionic with a positive charge on the nickel unit and an anionic charge on the borate unit, its nickel center nonetheless appears to be appreciably less electrophilic than in the more conventional cation $[(CH_3C(CH_2PPh_2)_3)NiI]^+$. This conclusion is consistent with other studies we have undertaken to resolve electronic differences between phosphine-supported zwitterions and their isostructural cations.[27] In general, the zwitterions appear to be more electron-rich by whichever measuring stick we use as a qualitative guide.

With complex **1** in hand, we prepared a series of complexes featuring other X-type ligands by metathetical routes to determine what geometries would be preferred for species of the general type [PhBP$_3$]NiX (Scheme 2**)**. For example, the yellow-green azide complex [PhBP$_3$]Ni(N$_3$) (**4**) can be prepared from sodium azide and exhibits a $\nu(N_3)$ vibration at 2060 cm^{-1} (KBr, C_6H_6), consistent with a terminal azide functionality that is corroborated by its solid-

(25) (a) Jenkins, D. M.; Di Billo, A. J.; Allen, M. J.; Betley, T. A.; Peters, J. C. *J. Am. Chem. Soc.* **2002**, *124*, 15336−15350. (b) Betley, T. A.; Peters, J. C. *Inorg. Chem.* **2003**, *42*, 5074−5084.

(26) Zanello, P.; Cinquantini, A.; Ghilardi, C. A.; Midollini, S.; Moneti, S.; Orlandini, A.; Bencini, A. *J. Chem. Soc., Dalton Trans.* **1990**, 3761−3766.

(27) (a) Thomas, J. C.; Peters, J. C. *J. Am. Chem. Soc.* **2003**, *125*, 8870−8888. (b) Thomas, J. C.; Peters, J. C. *J. Am. Chem. Soc.* **2001**, *123*, 5100−5101.

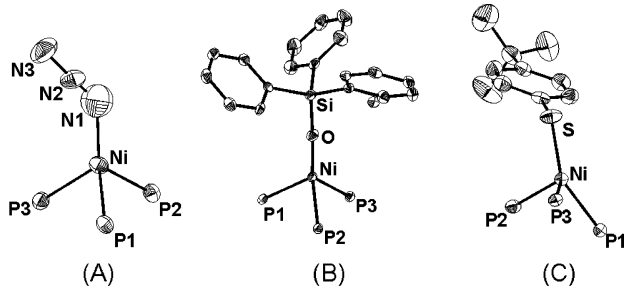

Figure 2. Molecular structures of (A) [PhBP$_3$]Ni(N$_3$) (**4**), (B) [PhBP$_3$]-Ni(OSiPh$_3$) (**5**), and (C) [PhBP$_3$]Ni(S-*p*-^{t}Bu-Ph) (**7**), derived from crystallographic studies. Only the L$_3$NiX subunit of each complex is represented. Complete structural details can be found in the Supporting Information. Selected interatomic distances (Å) and angles (deg) for **4**: Ni−N1, 1.915(12); Ni−P1, 2.262(2); Ni−P2, 2.261(2); Ni−P3, 2.255(2); P1−Ni−P2, 95.09(7); P1−Ni−P3, 90.80(8); P2−Ni−P3, 91.67(6); P1−Ni−N1, 126.7(4); P2−Ni−N1, 121.1(3); P3−Ni−N1, 122.4(4). For **5**: Ni−O, 1.820-(2); Ni−P1, 2.275(1); Ni−P2, 2.270(1); Ni−P3, 2.281(1); P1−Ni−P2, 89.77(3); P1−Ni−P3, 94.06(3); P2−Ni−P3, 91.65(3); P1−Ni−O, 123.59(8); P2−Ni−O, 89.77(3); P3−Ni−O, 130.20(8); Ni−O−Si, 168.08(14). For **7**: Ni−S, 2.119(1); Ni−P1, 2.189(1); Ni−P2, 2.188(1); Ni−P3, 2.244(1); P1−Ni−P2, 89.44(3); P1−Ni−P3, 91.28(3); P2−Ni−P3, 107.87(3); P1−Ni−S, 151.84(3); P2−Ni−S, 109.79(3); P3−Ni−S, 101.54(3).

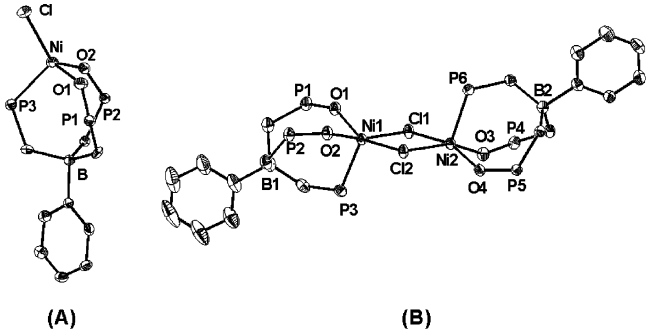

Figure 3. Displacement ellipsoid representation (50%) of (A) [PhB(CH$_2$P-(O)Ph$_2$)$_2$(CH$_2$PPh$_2$)]NiCl (**8A**) and (B) {[PhB(CH$_2$P(O)Ph$_2$)$_2$(CH$_2$PPh$_2$)]-NiCl}$_2$ (**8B**). Hydrogen atoms, phosphine phenyl rings, and solvent molecules have been omitted for clarity. Selected bond distances (Å) and angles (deg) for **8A**: Ni−Cl, 2.210(1); Ni−O1, 1.926(2); Ni−O2, 1.958(2); Ni−P3, 2.294(1); O1−Ni−O2, 98.79(7); O1−Ni−P3, 105.28(5); O2−Ni−P3, 97.64(5); O1−Ni−Cl, 116.74(5); O2−Ni−Cl, 125.31(5); P3−Ni−Cl, 110.07(3). For **8B**: Ni1−Cl1, 2.3543(11); Ni1−Cl2, 2.3814(12); Ni2−Cl1, 2.3311(12); Ni2−Cl2, 2.3916(11); Ni1−O1, 2.005(3); Ni1−O2, 1.989(3); Ni2−O3, 2.006(2); Ni2−O4, 1.980(3); Ni1−P3, 2.3125(13); Ni2−P6, 2.3236(13).

state molecular structure.[28] The molecular geometry of **4**, depicted in Figure 2, is monomeric and best described as pseudotetrahedral.[29] To our knowledge, **4** represents the only example of a crystallographically characterized nickel azide complex in which the azide ligand is coordinated to a single tetrahedral or pseudotetrahedral nickel center. Other nickel azides supported by sterically hindered tris(pyrazolyl)borate ligands have been prepared that present tetrahedral or five-coordinate structures in which the azide bridges two nickel centers.[30]

The green siloxide ([PhBP$_3$]Ni(OSiPh$_3$), **5**), the purple aryloxide ([PhBP$_3$]Ni(O-*p*-^{t}Bu-Ph), **6**), and the red arylthiolate ([PhBP$_3$]Ni(S-*p*-^{t}Bu-Ph), **7**) are all conveniently prepared by transmetalation with thallium reagents. The molecular structures of **5** and **7** are shown in Figure 2. The structure of **5** is related to its recently reported cobalt congener [PhBP$_3$]Co(OSiPh$_3$).[31] The Ni−O−Si bond angle of 168.08(14)° compares well with the Co−O−Si angle of 172.5(1)°. Perhaps structurally more interesting is the red thiolate complex **7**. A large number of nickel thiolates have been prepared, and their chemistry is of increasing interest due to their likely role in biocatalytic systems such as NiFe hydrogenase.[32] Four-coordinate nickel complexes that feature a single Ni−thiolate linkage remain quite rare, and to our knowledge all such examples that have been characterized are low spin and exhibit a square planar geometry.[33] The geometry of paramagnetic **7** (Evans method (C_6D_6, 298 K): $\mu_{eff} = 3.02\ \mu_B$) lies somewhere between a severely distorted tetrahedral structure type and a cis-divacant octahedron. Most striking is the dramatic variation in its three P−Ni−S bond angles, one of which is very large (151.84(3)°) and the other two (107.87(3)° and 109.79(3)°) of which are much closer to those of an idealized tetrahedron. Also of note is that the average Ni−P bond lengths of **7** (av 2.21 Å) are appreciably shorter than for **2** (av 2.27 Å), **4** (av 2.26 Å), and **5** (av 2.28 Å). Although the solid-state structure of aryloxide **6** has not been determined, we note that its paramagnetic ^{1}H NMR resonances in benzene-d_6 are very similar to those observed for **7**, suggesting that they have similar solution (and presumably solid-state) conformations.

The divalent [PhBP$_3$]NiX complexes **1**−**7** are all quite sensitive to dioxygen. While this reactivity has not been studied explicitly for each case, the product of the reaction of **1** with dioxygen has been determined. Thus, exposure of **1** to an excess of O_2 in benzene results in a rapid color change from green to purple. This color change is accompanied by a new and intense ν(P═O) vibration in the IR spectrum (1320 cm^{-1}) confirming a ligand oxidation reaction. We have observed this type of reactivity for tris(phosphino)borate-supported Fe(II) and Co(II) systems previously.[25] The nickel oxidation product was isolated as purple crystals at room temperature by vapor diffusion of petroleum ether into a benzene solution. XRD analysis of a representative single crystal established the monomeric and four-coordinate nickel complex [PhB(CH$_2$P(O)Ph$_2$)$_2$(CH$_2$PPh$_2$)]NiCl (**8A**) (eq 1 and Figure 3A), in which two of the phosphine donors have been oxidized to their corresponding phosphine oxides. Curiously, yellow rather than purple crystals are obtained if petroleum

(28) Nakamato, K. *Infrared and Raman Spectra of Inorganic and Coordination Compounds. Part B: Applications in Coordination, Organometallic, and Bioinorganic Chemistry*, 5th ed.; John Wiley & Sons: New York, 1997; pp 105−126.
(29) The structure of **4** suffers from modest disorder along its Ni−azide bond vector, and the thermal ellipsoid of the azide N atom directly linked to the nickel center is consequently quite large (see Supporting Information).
(30) Trofimenko, S.; Calabrese, J. C.; Kochi, J. K.; Wolowiec, S.; Hulsbergen, F. B.; Reedijk, J. *Inorg. Chem.* **1992**, *31*, 3943−3950.
(31) Jenkins, D. M.; Peters, J. C. *J. Am. Chem. Soc.* **2003**, *125*, 11162−11163.
(32) (a) Volbeda, A.; Charon, M.-H.; Piras, C.; Hatchikian, E. C.; Frey, M.; Fontescilla-Camps, J. C. *Nature* **1995**, *373*, 580−587. (b) Sellmann, D.; Geipel, F.; Moll, M. *Angew. Chem., Int. Ed.* **2000**, *39*, 561−563.
(33) (a) Sánchez, G.; Ruiz, F.; Serrano, J. L.; Ramírez de Arellano, M. C.; López, G. *Eur. J. Inorg. Chem.* **2002**, 2185−2191. (b) Clegg, W.; Henderson, R. A. *Inorg. Chem.* **2002**, *41*, 1128−1135. (c) Tucci, G. C.; Holm, R. H. *J. Am. Chem. Soc.* **1995**, *117*, 6489−6496. (d) Krüger, H.-J.; Holm, R. H. *Inorg. Chem.* **1989**, *28*, 1148−1155. (e) Kanatzidis, M. G. *Inorg. Chim. Acta* **1990**, *168*, 101−103.

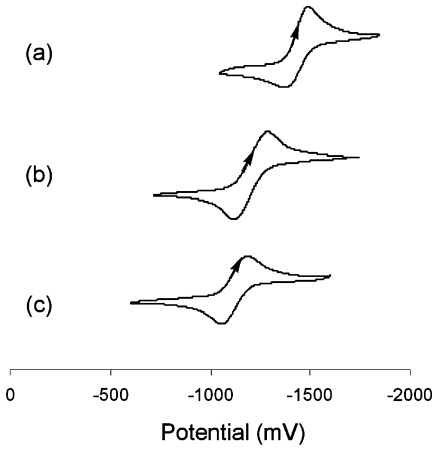

Figure 4. Cyclic voltammograms of (a) **3**, (b) **1**, and (c) **2** recorded at a scan rate of 100 mV/s in THF with Bu_4NPF_6 as the supporting electrolyte. Potentials are referenced to Fc/Fc^+.

ether is allowed to diffuse into a toluene solution of the oxidation product at *low temperature* (−40 °C). XRD analysis of a representative yellow crystal establishes the dimeric form of the oxidized chloride, {[PhB($CH_2P(O)Ph_2$)$_2$(CH_2PPh_2)]NiCl}$_2$ (**8B**), in which each of the chloride ligands now resides in a bridging position (Figure 3B). The structure of **8B** suffers from several disordered solvent molecules in the lattice; however, the dimeric nickel molecule is well-defined. The two structures intimate that monomeric **8A** is in equilibrium with its dimeric partner **8B** and that the equilibrium likely shifts in favor of the dimer at lower temperatures. A similar temperature dependent monomer/dimer equilibrium has been observed for the Ni(II) complex dichloro[bis(3,5-dimethylpyrazolyl)methane]Ni.[34]

$$\underset{\mathbf{1}}{[PhBP_3]NiCl} \xrightarrow[\text{benzene}]{\text{excess } O_2} \underset{\mathbf{8A} \text{ or } \mathbf{8B}}{\{[PhB(CH_2P(O)Ph_2)_2(CH_2PPh_2)]NiCl\}} \quad (1)$$

IIb. Electrochemical Data for Divalent Complexes. The tris(phosphino)borate ligands [$PhBP_3$] and [$PhBP^{iPr}_3$] effectively stabilize monovalent iron and cobalt complexes that prove to be effective precursors for the installation of multiple bond linkages via oxidative group transfer.[14−16] To determine the accessibility of monovalent nickel species we first studied the cyclic voltammetry of the divalent nickel precursors. These studies were performed in THF using [^{n}Bu$_4$N][PF_6] (0.35 M) as the supporting electrolyte. All data were referenced to Fc/Fc^+ as an internal standard using $Ag/AgNO_3$ as the reference electrode.

Figure 4 compares the first reduction process observed for the halide complexes **1**, **2**, and **3**. Each process is assigned as a one-electron reduction of $L_3Ni^{II}X$ to $[L_3Ni^{I}X]^-$. A fully reversible reduction process is observed for the chloride complex **1** at −1.20 V (Figure 4b). The $Ni^{II/I}$ couple shifts to −1.12 V (Figure 4c) upon replacement of chloride by the weaker field iodide ligand in **2**. The cyclic voltammetry of **3** shows a quasi-reversible redox process (100 mV/s) at an appreciably lower potential (−1.44 V, Figure 4a). An increase in the solution concentration of **3** ($\geq 1 \times 10^{-3}$ M) resulted in rapid deposition of material on the glassy carbon electrode and the disappearance of the reduction wave. The $Ni^{II/I}$ couple for **3** as compared to **1** ($\Delta E_{1/2} = 240$ mV) reflects an appreciable difference in electron-releasing character of the [$PhBP^{iPr}_3$] ligand relative to its [$PhBP_3$] counterpart. This distinction is consistent with the cyclic voltammograms obtained previously for the complexes [$PhBP^{iPr}_3$]FeCl and [$PhBP_3$]FeCl ($\Delta E_{1/2} = 322$ mV).[15,25b] Important to note is that the cyclic voltammograms for complexes **1**, **2**, and **3** do not provide any evidence for an oxidation wave within the detectable range (i.e., below ∼1.0 V).

It is interesting to compare these data to those of several other $L_3Ni^{II}X$ systems that have been characterized electrochemically. For example, the cationic tripodal phosphine system [($CH_3C(CH_2PPh_2)_3$)NiX][ClO_4] has been examined previously and shows a fully reversible $Ni^{II/I}$ redox processes at −0.53 V (X = Cl) and −0.43 V (X = I) in CH_2Cl_2 solution relative to Fc/Fc^+.[26,35] The $Ni^{II/I}$ couple is thus shifted approximately 700 mV positive on translating from the neutral $L_3Ni^{II}X$ structure type to the isostructural but cationic $L_3Ni^{II}X^+$ structure type. The magnitude of the difference in redox couples between the two systems seems large given the zwitterionic nature of the neutral [$PhBP_3$]NiX system. An appreciable difference in the degree of solvent reorganization upon oxidation is to be expected, and this difference, coupled with the increased electron-richness we expect for zwitterionic systems supported by (phosphino)borates, suggests that a relatively large difference in redox potentials is in fact quite reasonable. Related infrared carbonyl model studies from our lab have comparatively examined electronic factors between zwitterions and their isostructural cations and revealed unexpectedly large differences in ν(CO) values between such systems, the zwitterions always giving rise to much lower CO frequencies.[36,37,54] It is also interesting to compare Riordan's tris(thioether)borate complex [PhTt$^{t\text{Bu}}$]NiCl ([PhTt$^{t\text{Bu}}$] = [PhB(CH_2S^tBu)$_3$]$^-$), which features an *irreversible* $Ni^{II/I}$ redox process at −1.3 V relative to Fc/Fc^+ in CH_2Cl_2.[38] The irreversible nature of its one electron reduction makes a direct comparison to the one electron reduction potentials of the [$PhBP_3$]NiX systems tenuous. It is nonetheless qualitatively interesting, and perhaps surprising, that the reduction potential for Riordan's sulfur-supported nickel system is approximately as low as the phosphine-supported [$PhBP_3$]Ni(II) complexes **1** and **2**.

The cyclic voltammetry of the [$PhBP_3$]NiX complexes (X = −OSiPh_3, **5**; −O-*p*-^{t}Bu-Ph, **6**; −S-*p*-^{t}Bu-Ph, **7**) was also studied between +1.2 and − 3.0 V to examine what effect X-type ligands of better π-donor strength might have on the Ni(II/I) redox process and to examine whether such ligands might better stabilize the Ni(III) oxidation state. As a point

(34) Reedijk, J.; Verbiest, J. *Transition Met. Chem.* **1978**, *3*, 51−52.

(35) The authors report potentials versus SCE and corrected these values relative to Fc/Fc^+.

(36) Betley, T. A.; Peters, J. C. *Inorg. Chem.* **2003**, *42*, 5074−5084.

(37) Betley, T. A.; Peters, J. C. *Angew. Chem., Int. Ed.* **2003**, *42*, 2385−2389.

(38) Schebler, P. J.; Riordan, C. G.; Guzei, I. A.; Rheingold, A. L. *Inorg. Chem.* **1998**, *37*, 4754−4755.

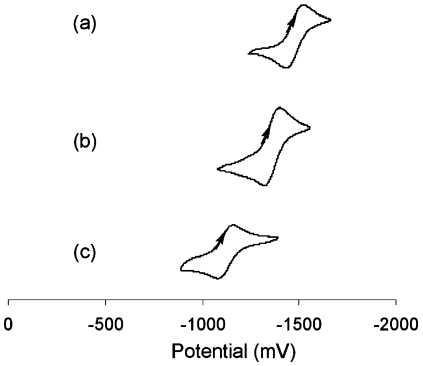

Figure 5. Cyclic voltammograms of (a) **5**, (b) **6**, and (c) **7** recorded at a scan rate of 100 mV/s. Potentials are referenced to Fc/Fc^{+}.

of reference, we have previously reported that the complex $[PhBP_3]Co(OSiPh_3)$ exhibits fully reversible $Co^{III/II}$ and $Co^{II/I}$ redox processes, but that its iodide counterpart $[PhBP_3]CoI$ exhibits only a single reversible redox couple ($Co^{II/I}$) along with an irreversible $Co^{III/II}$ oxidation wave.[25b,31] Reversible $Ni^{II/I}$ reduction processes are observed for each of the complexes **5**, **6**, and **7** (Figure 5). The siloxide complex **5** exhibits the most negative potential at −1.47 V (Figure 5a). Like its cobalt relative, complex **5** also exhibits an oxidation wave at higher potential (0.350 V), but in this case the process is irreversible. Its irreversibility suggests that the putative $[Ni^{III}-OSiPh_3]^{+}$ species generated decays rapidly under these conditions. A similar set of observations was made for the aryloxide complex **6**. It exhibits a single and reversible reduction process ($Ni^{II/I}$) at −1.36 V (Figure 5b), and an irreversible oxidation event at 0.240 V, suggesting that complex **6** is both easier to reduce and easier to oxidize than the siloxide complex **5**. The arylthiolate complex **7** displays the most readily accessible $Ni^{II/I}$ redox couple (−1.12 V, Figure 5c). Perhaps more interesting is that **7** also shows a second reduction event at −2.56 V. This latter process is irreversible, and while we suspect that it corresponds to a $Ni^{I/0}$ redox change, it may also represent a reduction event at the arylthiolate ligand. As discussed below, the Ni(0) state is more readily accessible within these BP_3Ni systems when π-acidic ligands are coordinated to the fourth binding site. Finally, an irreversible oxidation event is observed at 0.170 V for **7**, establishing that it is more easily oxidized than either **5** or **6**. Considered collectively, these electrochemical data establish that monovalent nickel is readily accessible within these BP_3Ni platforms, but that the stabilization of a trivalent nickel state is likely to require more strongly π-donating X-type ligands.

IIc. Chemical Reduction of $[PhBP_3]NiX$ and $[PhBP^{iPr}_3]$-NiCl Precursors. Given the electrochemical stability of monovalent nickel within these P_3NiX platforms, it was of interest to investigate the preparation of Ni(I) complexes for subsequent group transfer studies. Efforts to prepare and study the reactivity patterns of molecular Ni(I) species have only recently been pursued in a systematic fashion. For instance, Hillhouse and co-workers have prepared a series of $L_2Ni^{I}X$ complexes that feature halides, pseudohalides, and alkyls as the X-type ligand using relatively soft phosphine donor ligands.[8−10] Riordan's group has moreover made use

Scheme 3

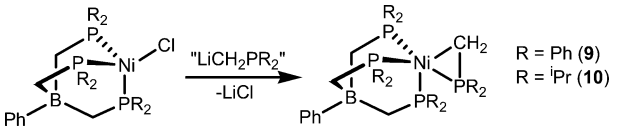

of rather soft tris(thioether)borate ligands to stabilize Ni(I). For example, the reduction of $[PhTt^{tBu}]NiCl$ by methyllithium under a blanket of CO produces the Ni(I) species $[PhTt^{tBu}]$-Ni(CO).[39] Ni(I) complexes species supported by betadiketiminate ligands have also been reported recently.[40]

The direct reduction of chloride **2** by Na/Hg in THF led to the generation of a diamagnetic red organometallic, $[PhBP_3]Ni(\eta^2\text{-}CH_2PPh_2)$ (**9**), rather than the anticipated $[PhBP_3]Ni^{I}Cl^{-}$ anion suggested by the cyclic voltammetry of **2**. The same product was formed when other strong reductants were examined, including sodium mirror and potassium graphite. Complex **9** can be synthesized independently in high yield by the direct reaction of **1** with $Ph_2PCH_2Li(TMEDA)$ (Scheme 3), and it appears to be a thermodynamic sink within the $[PhBP_3]Ni$ system. For instance, when potentially reducing nucleophiles, such as alkyllithiums or lithium amides, are added to chloride **2** at low temperature (−78 °C), complex **9** is invariably generated as the dominant reaction product. Riordan's $[PhTt^{tBu}]NiCl$ system was reported to behave in a similar fashion in the presence of alkyllithiums without a trapping ligand such as CO or PMe_3 available.[39] An obvious unanswered question for both systems concerns whether (i) a bona fide $Ni^{II}-$alkyl (or $Ni^{II}-$amide) is generated but is inherently unstable within these pseudotetrahedral borate-based systems and somehow degrades to **9** or (ii) outer-sphere electron transfer occurs as a first step to generate $L_3Ni^{I}-Cl^{-}$, which is unstable to chloride loss and subsequent degradation to **9**. At present we can only conclude that complexes **1** and **2** are sensitive to reducing conditions, and that borate ligand degradation can occur even at low temperatures to produce **9**. Degradation processes are less problematic when a donor ligand trap is used (vide infra).

A reaction worthy of particular comment is that between $CoCp_2$ and **1** in the presence of $[^{n}Bu_4N][PF_6]$. The crude product of this reaction is a new paramagnetic species (^1H NMR) that is tentatively formulated as the one electron reduced complex $\{[PhBP_3]Ni^{I}Cl\}\{^{n}Bu_4N\}$. This species is very unstable in solution and has not been isolated in analytically pure form. Solution degradation occurs to produce a mixture of both paramagnetic and diamagnetic products even at low temperatures (−40 °C). Nonetheless, its assignment is consistent with the following observation: rapid reoxidation of the crude product using $[Fc][PF_6]$ regenerates the starting nickel halide **1** in ∼85% yield (^1H NMR).

The related reduction chemistry of $[PhBP^{iPr}_3]NiCl$ (**3**) with a variety of typical reductants, for example, Na/Hg, sodium

(39) Schebler, P. J.; Mandimutsira, B. S.; Riordan, C. G.; Liable-Sands, L. M.; Incarvito, C. D.; Rheingold, A. L. *J. Am. Chem. Soc.* **2001**, *123*, 331−332.
(40) Holland, P. L.; Cundari, T. R.; Perez, L. L.; Eckert, N. A.; Lachicotte, R. J. *J. Am. Chem. Soc.* **2002**, *124*, 14416−14424.

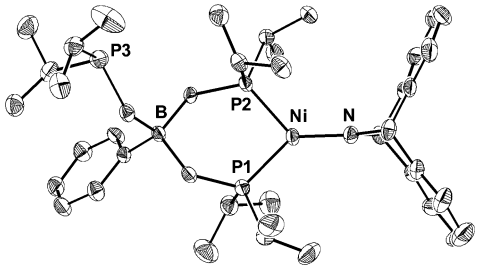

Figure 6. Displacement ellipsoid representation (50%) of [κ^2-PhBP^{i}Pr$_3$]Ni(dbabh) (**11**). Hydrogen atoms have been omitted for clarity. Selected distances (Å) and angles (deg): P1−Ni, 2.1475(7); P2−Ni, 2.1317(7); N−Ni, 1.748(2); P1−Ni−P2, 93.38(3); P1−Ni−N, 136.86(7); P2−Ni−N, 129.65(7).

naphthalenide, potassium graphite, Mg^0, and (9,10-dihydro-9,10-anthracenediyl)tris(tetrahydrofuran)magnesium, was also surveyed. These reactions *did not* result in the formation of the degradation product [PhBP$^{iPr}_3$]Ni(η^2-CH$_2$P^{i}Pr$_2$) (**10**), which was synthesized independently by reaction of **3** with LiCH$_2$P^{i}Pr$_2$ in THF (Scheme 3). Ill-defined product mixtures resulted instead.

The [PhBP$^{iPr}_3$] anion lowers the reduction potential of the divalent nickel state considerably as observed in our electrochemical studies, and we therefore suspected that [PhBP$^{iPr}_3$]-NiCl might give rise to cleaner substitution chemistry with potentially reducing nucleophiles rather than problematic redox chemistry. The reactivity of **3** was therefore explored with a host of lithiated amines. One example concerns the lithium amide Li(dbabh) (Hdbabh = 2,3:5,6-dibenzo-7-azabicyclo[2.2.1]hepta-2,5-diene),[41] chosen as a possible N-atom transfer reagent (vide infra). The reaction between **3** and Li(dbabh) at low temperature results in an inky green-brown solution from which the three-coordinate nickel(II) complex [κ^2-PhBP$^{iPr}_3$]Ni(dbabh) (**11**) can be isolated. The three coordinate nature of **11** in solution is strongly suggested by its NMR data, which shows a diamagnetic product. Interestingly, only one phosphine environment is evident by both ^{1}H NMR and ^{31}P{^{1}H} NMR spectroscopy, indicative that the phosphine ligands of **11** are in rapid exchange. Definitive assignment of the structure of **11** is provided by its solid-state molecular structure (Figure 6). As can be seen, the amide ligand adopts a conformation such that its available π-orbital lies in the P$_2$Ni plane. This conformation is similar to a related (dtbpe)Ni−NR$_2$ species (dtbpe = ^{t}Bu$_2$PCH$_2$-CH$_2$P^{t}Bu$_2$) prepared by the Hillhouse group.[8] When comparing **11** to other Ni−amide complexes, it is interesting to note that most of their Ni−N distances range from 1.82 to 1.93 Å,[42] approximately 0.1 Å longer than that observed for **11**. The Ni−N distance of **11** (1.748(2) Å) is quite similar, however, to that reported for [(dtbpe)Ni−NH{2,6-(CHMe$_2$)$_2$C$_6$H$_3$}][PF$_6$] (1.768(14) Å).[8] The short Ni−N bond length suggests a significant π-interaction, consistent with the orientation of the amide ligand. The dechelation of one phosphine ligand in **11** is likely favored due to this π-interaction. In addition to Li(dbabh), the reaction between **3** and lithium anilides, such as Li(NHPh) and Li{NH(2,6-diisopropylphenyl)}, also suggests the formation of three coordinate Ni^{II}−NR$_2$ structures. These products are likewise diamagnetic and give highly colored solutions (red and purple, respectively). It appears that the [PhBP$^{iPr}_3$]Ni^{II} scaffold is more resistant to outer-sphere reduction and thereby allows cleaner substitution to occur at the Ni(II) state. However, the pseudotetrahedral geometry is compromised by dechelation of one phosphine donor.

(41) Mindiola, D. J.; Cummins, C. C. *Angew. Chem., Int. Ed.* **1998**, *37*, 945−947.
(42) See ref 8 and references therein.

Scheme 4

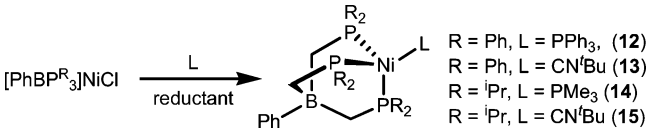

IId. Synthesis and Characterization of [PhBP$_3$]Ni^{I}L and [PhBP$^{iPr}_3$]Ni^{I}L Complexes. The presence of a suitable L-type trapping ligand can stabilize the Ni(I) state to give synthetically useful precursors (Scheme 4). For example, the reduction of **1** in the presence of PPh$_3$ by KC$_8$ yields [PhBP$_3$]-Ni(PPh$_3$) (**12**) in good yield. PMe$_3$ is also an effective trap. The core structure of **12** is shown in Figure 7. Similarly, the reduction of **1** by sodium amalgam in the presence of ^{t}BuNC results in the formation of [PhBP$_3$]Ni(CN^{t}Bu) (**13**). It is observed that the addition of ^{t}BuNC to **1** prior to addition of the reductant causes an immediate color change from green to purple. NMR spectra of the purple reaction mixture (^{1}H and ^{31}P{^{1}H}) show the formation of a diamagnetic intermediate prior to reduction, presumably "[κ^2-PhBP$_3$]Ni(Cl)(CN^{t}Bu)". Complexes **12** and **13** are paramagnetic and exhibit solution magnetic moments of 1.91 μ_B and 1.74 μ_B, respectively. Complex **13** exhibits an intense ν(CN) band in its IR spectrum at 2094 cm^{-1} (KBr, C$_6$H$_6$) suggesting that the isocyanide ligand is terminal.[28] This is corroborated by its solid-state molecular structure (Figure 7).

The [PhBP$^{iPr}_3$]NiCl (**3**) precursor can be similarly reduced to form P$_3$Ni^{I}L complexes (Scheme 4). Reduction of **3** using a sodium/mercury amalgam in the presence of excess PMe$_3$ (5 equiv) results in the formation of analytically pure bright yellow [PhBP$^{iPr}_3$]Ni(PMe$_3$) (**14**). Yellow **14** is also formed in good yield from the reaction of the Ni(0) precursor Ni(PMe$_3$)$_4$ with [PhBP$^{iPr}_3$]Tl. This reaction proceeds with concomitant reduction of Tl(I) to Tl(0), evident by the precipitation of thallium metal from solution. Crystals of **14** were obtained from this latter reaction by crystallization from diethyl ether at −30 °C. XRD analysis showed that the crystals contained a 95:5 mixture of **14** and [PhBP$^{iPr}_3$]Tl. The presence of a small amount of [PhBP$^{iPr}_3$]Tl in the crystals was also visible from their ^{31}P{^{1}H} NMR spectrum and by the presence of a well-refined peak in the difference Fourier map attributable to the presence of thallium (see Supporting Information for refinement details). The molecular structure of **14**, depicted in Figure 7, shows a four-coordinate and pseudotetrahedral Ni(I) center very similar to that for **12**. Measurement of the magnetic moment of analytically pure **14** by the method of Evans in benzene solution provides μ_{eff} = 1.82 μ_B, consistent with one unpaired electron for the d^9 electronic configuration. A [PhBP$^{iPr}_3$]-ligated Ni(I) isocyanide complex has also been prepared by a similar method.

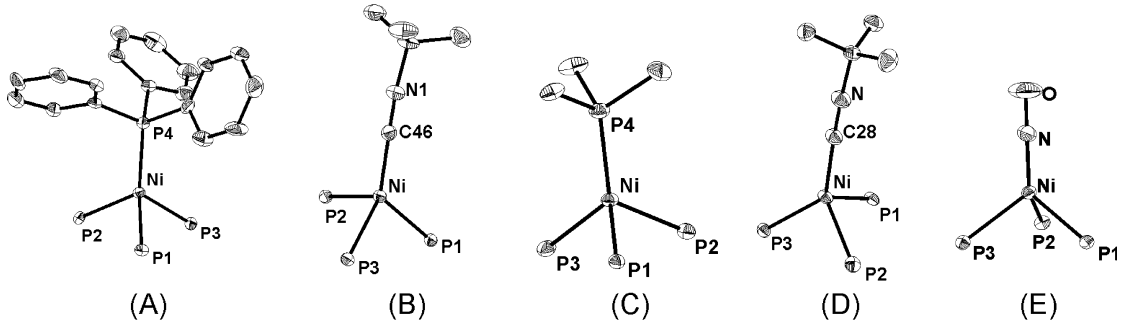

Figure 7. Molecular structures of (A) [$PhBP_3$]Ni(PPh_3) (**12**), (B) [$PhBP_3$]Ni(CN^tBu) (**13**), (C) [$PhBP^{iPr}_3$]Ni(PMe_3) (**14**), (D) [$PhBP^{iPr}_3$]Ni(CN^tBu) (**15**), and (E) [$PhBP_3$]NiNO (**16**), derived from crystallographic studies. Only the L_3NiX subunit of each complex is represented. Complete structural details can be found in the Supporting Information. Selected interatomic distances (Å) and angles (deg) for **12**: Ni−P1, 2.28(2); Ni−P2, 2.28(2); Ni−P3, 2.27 (2); Ni−P4, 2.25(2); Ni−B, 3.44(9); P1−Ni−P4, 120.1(8); P2−Ni−P4, 122.1(8); P3−Ni−P4, 123.0(8); P1−Ni−P2, 95.6(8); P2−Ni−P3, 96.8(8); P1−Ni−P3, 92.2(8). For **13**: Ni−C46, 1.861(2); Ni−P1, 2.229(1); Ni−P2, 2.216(1); Ni−P3, 2.252(1); P1−Ni−P2, 91.86(2); P1−Ni−P3, 95.00(2); P2−Ni−P3, 94.58(2); P1−Ni−C46, 125.59(6); P2−Ni−C46, 107.38(6); P3−Ni−C46, 131.77(6). For **14**: Ni−P1, 2.2533(5); Ni−P2, 2.2764(5); Ni−P3, 2.2873(5); Ni−P4, 2.2631(5); Ni−B, 3.436(2); P1−Ni−P4, 118.67(2); P2−Ni−P4, 121.90(2); P3−Ni−P4, 123.43(2); P1−Ni−P2, 92.76(2); P2−Ni−P3, 98.24(2); P3−Ni−P1, 94.74(2). For **15**: Ni−C28, 1.864(2); Ni−P1, 2.2403(5); Ni−P2, 2.2749(6); Ni−P3, 2.2562(6); Ni−B, 3.431(2); P1−Ni−P2, 96.83(2); P1−Ni−P3, 93.50(2); P2−Ni−P3, 96.42(2); P1−Ni−C28, 104.56(6); P2−Ni−C28, 124.37(7); P3−Ni−C28, 131.79(7). For **16**: Ni−N, 1.624(3); N−O, 1.183(3); Ni−P1, 2.232(1); Ni−P2, 2.215(1); Ni−P3, 2.234(1); O−N−Ni, 176.0(3); P1−Ni−P2, 92.54(3); P1−Ni−P3, 95.42(3); P2−Ni−P3, 91.74(3); P1−Ni−N, 124.68(9); P2−Ni−N, 119.84(9); P3−Ni−N, 124.01(9).

Addition of excess (ca. 5 equiv) ^{t}BuNC to **3** in THF solution results in the initial formation of a red, likely square planar Ni(II) complex, [κ^2-$PhBP^{iPr}_3$]Ni(Cl)(CN^tBu) (**19**). Assignment of this species is based upon its $^{31}P\{^1H\}$ NMR spectrum (δ 62.7 (br d), 47.7 (br d), 3.2 (br s)). Removal of the reaction volatiles followed by redissolution in THF and subsequent reduction using sodium/mercury amalgam provides the yellow Ni(I) complex [$PhBP^{iPr}_3$]Ni(CN^tBu) (**15**) in good yield. Attempts to reduce **3** in the presence of excess CN^t-Bu result in the formation of an increased number of side products, presumably due to the competitive reduction of isocyanide. Complex **15** is more readily prepared in high yield by the reaction of **14** with excess (ca. 5 equiv) CN^tBu, which substitutes PMe_3. The solution magnetic moment of **15** as determined by the Evans method is 1.68 μ_B. Examination of the IR spectrum of **15** provides a ν(CN) stretching frequency of 2056 cm^{-1} (KBr, THF). The increased electron-releasing character of [$PhBP^{iPr}_3$] versus [$PhBP_3$] is quite striking from the ν(CN) vibrations recorded for **15** and **13**, the former being shifted to lower energy by 38 cm^{-1}. The relatively similar solid-state structures of **15** and **13** are evident in Figure 7. Hence, this electronic comparison is a good qualitative benchmark for the [$PhBP^{iPr}_3$] and [$PhBP_3$] anions. To the best of our knowledge, complexes **13** and **15** are the only structurally characterized, mononuclear Ni(I) isocyanide complexes.

IIe. Access to the Ni(0) State. With Ni(I) complexes in hand, we studied their proclivity to undergo redox events by electrochemical methods. The cyclic voltammetry of the Ni(I) complexes **14** and **15** was studied in THF solution. The cyclic voltammetry of **14** shows a reversible reduction to Ni(0) at −1945 mV (Figure 8b). An irreversible oxidation event occurs at −503 mV. **15** gives rise to a low reduction potential for the $Ni^{I/0}$ couple (−1848 mV) (Figure 8a), and an irreversible oxidation event (−396 mV). The shift to more positive potentials for both the oxidation and reduction processes for **15** as compared to **14** reflects the exchange of an electron-donating phosphine ligand for a π-acidic isocyanide ligand. Both complexes show reduction processes, presumably to Ni(0), at quite low potentials.

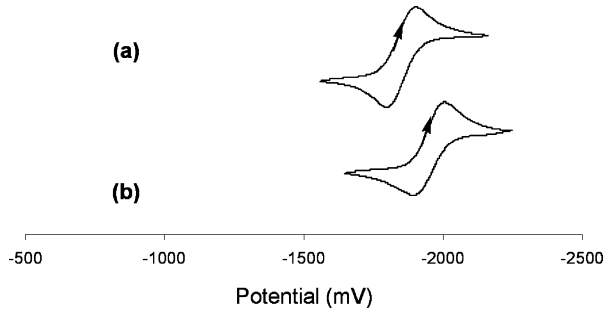

Figure 8. Cyclic voltammograms of (a) **15** and (b) **14** recorded at a scan rate of 50 mV/s. Potentials are referenced to Fc/Fc^+.

On the basis of these electrochemical observations, we studied the independent chemical reduction of [$PhBP^{iPr}_3$]Ni(PMe_3) (**14**). As suggested from the formation of **14** by the reaction between [$PhBP^{iPr}_3$]Tl and $Ni(PMe_3)_4$, the putative Ni(0) anion {[$PhBP^{iPr}_3$]Ni(PMe_3)}$^-$ (**20**) is generated at very low potential. Anionic {[$PhBP^{iPr}_3$]Ni(PMe_3)}$^-$ appears to be accessible by reduction of **14** with strong alkali metal reductants, such as Na/Hg or KC_8, in THF solution. Examination of the ^{1}H NMR spectra of such reduction reactions shows complete consumption of paramagnetic **14** and the presence of broadened diamagnetic resonances consistent with a fluxional Ni(0) anion. In THF solution, these complexes have limited stability and ultimately reoxidize to Ni(I) **14**.

The reduction chemistry of neutral [$PhBP^{iPr}_3$]Ni(CN^tBu) **15** was also studied. Chemical reduction of **15** using strong reductants (e.g., KC_8, Na/Hg) results in its complete consumption and the formation of a diamagnetic species (^{1}H NMR). The solution infrared spectrum of this product shows a dramatically shifted ν(CN) vibration (1982 cm^{-1}, compared with 2056 cm^{-1} for **15**), indicating the presence of the Ni(0) anion {[$PhBP^{iPr}_3$]Ni(CN^tBu)}$^-$ (**21**). This species is kinetically unstable in benzene or THF solution and gradually decays to regenerate the Ni(I) species **15** as the predominant

product. Whether some type of disproportionation reaction or reaction with solvent occurs is presently unclear. The degradation process to regenerate **15** is quite clean, suggesting the involvement of some external electron acceptor such as THF solvent.

Synthetic access to other zerovalent nickel species supported by these phosphine anions is possible.[43] For example, treatment of **1** with NO gas generates the diamagnetic nitrosyl product [$PhBP_3$]Ni(NO) (**16**) as a crystalline red product (eq 2). This complex is formally an 18-electron species and is isolobal to its well-known relatives CpNi(NO)[44] and Cp*Ni(NO).[45] The solid-state structure of **16** (Figure 7) shows a pseudotetrahedral nickel complex with a nearly linear Ni−N−O bond angle (176.0(3)°) and a very short Ni−N bond distance of 1.624(3) Å. Complex **16** also exhibits a rather low ν(NO) vibration at 1737 cm^{-1} (KBr, C_6H_6), considerably lower than observed for the tris(thioether)borate system [$PhTt^{tBu}$]Ni(NO) (1785 cm^{-1}, CH_2Cl_2)[38] and the Cp* system Cp*Ni(NO) (1787 cm^{-1}, Nujol).[46] Another structurally related example is Sacconi's four-coordinate nickel nitrosyl [(κ^3(P)-np_3)Ni(NO)][BPh_4] (np_3 = $N(CH_2CH_2PPh_2)_3$).[47] The average of the P−Ni bond distances in [(κ^3(P)-np_3)Ni(NO)]-[BPh_4] is 2.293(6) Å, and its Ni−NO bond distance is 1.59(2) Å. Thus, all of the Ni−ligand linkages contract for the cation [(np_3)Ni(NO)]$^+$ by comparison to **16**. Cationic [(κ^3(P)-np_3)-Ni(NO)][BPh_4] displays a ν(NO) at 1755 cm^{-1} (Nujol), intermediate between those for **16** and [$PhTt^{tBu}$]Ni(NO) or Cp*Ni(NO). The remarkably low ν(NO) frequency recorded for **16** indicates a very large degree of π-back-bonding and is perhaps suggestive that the Ni=N=O resonance contributor is meaningful. The N−O bond distance of 1.183(3) Å is nonetheless similar to those recorded in the other structures.

$$\mathbf{1} \text{ or } \mathbf{12} \xrightarrow{NO} \underset{\mathbf{16}}{[PhBP_3]Ni(NO)} \qquad (2)$$

Access to Ni(0) carbonyl complexes was achieved by reaction of either of the tris(phosphino)borate ligands with $(Ph_3P)_2Ni(CO)_2$. Thus, the anionic complex [[κ^2-$PhBP_3$]Ni-$(CO)_2$][$^nBu_4N$] (**17**) is synthesized cleanly by the reaction between [$PhBP_3$]Tl and $(Ph_3P)_2Ni(CO)_2$ in the presence of [$^nBu_4N$][Br] in THF over a period of 12 h. Its $^{31}P\{^1H\}$ NMR spectrum shows two distinct resonances at 29.2 and −9.46 ppm (2:1 ratio) that correspond to its coordinated and dissociated phosphine donors, respectively. The solution IR spectrum of this complex (KBr, THF) shows symmetric and antisymmetric ν(CO) vibrations at 1994 and 1913 cm^{-1}. Synthesis of the analogous [$PhBP^{iPr}_3$]-containing complex is achieved by reaction of [$PhBP^{iPr}_3$]Tl with $(Ph_3P)_2Ni(CO)_2$ in the presence of ASNBr (ASN = 5-azoniaspiro[4.4]nonane) in THF solution. The substitution reaction is much slower in the latter case, but proceeds in reasonable yield after a period of 3 days at room temperature to form [[κ^2-$PhBP^{iPr}_3$]-$Ni(CO)_2$][ASN] (**18**). Attempts to accelerate the reaction via mild heating (50 °C) result in extensive decomposition of the starting material to unidentified products. Complex **18** displays a characteristic infrared spectrum (2004 (sym) and 1878 cm^{-1} (antisym); KBr, THF) and $^{31}P\{^1H\}$ NMR spectrum (δ 51.1 (s, 2P), 4.8 (s, 1P)). Photolysis of **17** under a sparge of N_2 appears to affect replacement of one of the CO ligands by the remaining phosphine donor to produce the κ^3 species {[$PhBP_3$]Ni(CO)}{$^nBu_4N$} (**22**). A single sharp resonance is observed in the $^{31}P\{^1H\}$ NMR spectrum for **22** at 25.3 ppm, and a single ν(CO) vibration is observed at 1869 cm^{-1} (KBr, THF). This value is comparable but appreciably lower than the ν(CO) value of 1890 cm^{-1} (Nujol) reported for the neutral Ni(0) complex (triphos)Ni(CO).[48] We were surprised to find that attempts to oxidize **17** and **18** by [Fc][PF_6] to give well-defined Ni(I) monocarbonyl products instead led to multiple products as determined by IR and NMR spectroscopy. Given the stability of Riordan's [$PhTt^{tBu}$]Ni^I(CO) and related Ni(I) carbonyls,[39] we suspect overoxidation to be problematic. Gentler oxidants may yet prove synthetically effective.

IIf. Synthetic Attempts To Generate Ni=E/Ni≡E Linkages. One of the primary goals of this study was to assess the propensity of the low valent nickel precursors described herein to mediate oxidative group transfer processes that install Ni=E/Ni≡E multiple bond linkages at a pseudotetrahedral nickel center. We have canvassed numerous reactions that might have led to such species, but to date have not isolated or spectroscopically verified well-defined examples of L_3Ni=E/L_3Ni≡E. It is nonetheless informative to briefly summarize these attempts.

One of the more interesting target molecules whose stability we sought to evaluate concerns the tetravalent L_3Ni^{IV}≡N. This hypothetical d^6 unit would be both isolobal and isoelectronic to remarkably stable d^6 L_3Co^{III}≡NR species that our lab has prepared previously.[14,16] It would moreover be structurally related to a recently reported d^4 L_3Fe^{IV}≡N system.[18] Various routes were canvassed to generate a putative Ni^{IV}≡N species, and two are most worthy of comment. Photolysis of the divalent azide **4** precursor might effect N_2 expulsion and thus nitride transfer to nickel to produce "[BP_3]Ni^{IV}≡N". We find, however, that the azide ligand remains intact even under extended photolysis (Hg lamp) in THF at room temperature. Extended heating of **4** results in a mixture of diamagnetic and paramagnetic products, but there was no spectroscopic evidence to suggest that any of these products correspond to a nitride functional group (bridging or terminal). Another plausible route to the terminal nitride concerns a two-electron oxidative N-atom transfer from the dbabh amide to Ni(II). Precedence for this type of transformation has been provided by Mindiola and

(43) For relevant reviews on the synthesis of transition metal nitrosyl complexes see: (a) Mingos, M. D.; Sherman, D. J. *Adv. Inorg. Chem.* **1989,** *34,* 293−377. (b) Richter-Addo, G. B.; Legzdins, P. *Metal Nitrosyls;* Oxford University Press: New York, 1992; pp 34−78.

(44) Crichton, O.; Rest, A. J. *J. Chem. Soc., Dalton Trans*. **1977**, 986−993.

(45) Schneider, J. J.; Goddard, R.; Krueger, C. *Organometallics* **1991**, *10*, 665−670.

(46) (a) Fomitchev, D. V.; Furlani, T. R.; Coppens, P. *Inorg. Chem*. **1998**, *37*, 1519−1526. (b) Green, J. C.; Underwood, C. *J. Organomet. Chem.* **1997**, *528*, 91−94.

(47) Di Vaira, M.; Ghilardi, C. A.; Sacconi, L. *Inorg. Chem.* **1976**, *15*, 1555−1561.

(48) Bianchini, C.; Mealli, C.; Meli, A.; Scapacci, G. *Organometallics* **1983**, *2*, 141−143.

Cummins in the synthesis of a $Cr^{VI}\equiv N$ nitride,[41] and more recently by our lab in the generation of $[PhBP^{iPr}_3]Fe^{IV}\equiv N$.[18] As described above, the reaction between Li(dbabh) and **3** installs the required $Ni^{II}-N$ amide linkage, but the thermodynamically stable product is the trigonal planar three-coordinate Ni^{II} species **11** rather than the four-coordinate complex. We had hoped that the $[PhBP^{iPr}_3]$ ligand might be sufficiently electron-releasing to induce the loss of anthracene with concomitant nitride transfer to generate the $Ni^{IV}\equiv N$ subunit. Dechelation of a phosphine arm occurs instead to give a relatively stable amide. Complex **11** is quite stable at room temperature in solution, and while its thermolysis at slightly elevated temperature does produce a new diamagnetic species, the ^1H NMR spectrum of the species definitively shows the presence of an intact dbabh ligand, evident from the signature bridgehead proton resonance (ca. 5.4 ppm). A definitive structural assignment for this thermolysis product has not yet been made.

By analogy to the previously reported reactions of $[BP_3]M^IL$ precursors (where $[BP_3] = [PhBP_3]$ and $[PhBP^{iPr}_3]$, M = Fe and Co, L = PR_3) with aryl and alkyl azide (RN_3) substrates to generate $M^{III}\equiv NR$ imides,[14,15] it was of obvious interest to canvass similar reactions with the low valent nickel precursors described herein. To this end, we surveyed a number of reactions that might have facilitated two-electron group transfer reactivity to install a Ni=NR linkage. The reaction of **12**, **13**, **14**, and **15** with 2 equiv of an organic azide (typical organic azides used: *p*-tolyl azide, *tert*-butyl azide, 1-adamantyl azide, tosyl azide, and trimethylsilyl azide) in each case produces a mixture of paramagnetic and diamagnetic species that is relatively ill-defined. The phosphine-capped Ni(I) complexes react relatively quickly at room temperature (hours). By contrast, the Ni(I) isocyanide complexes reacted much more slowly. In these latter cases, starting material is still present even after several days at room temperature. Attempts to accelerate the rate of these reactions by heating reaction mixtures of **13** and **15** in the presence of azide substrates did lead to more rapid consumption of the nickel precursors, but also to an even greater range of spectroscopically detectable species. A major organic product of the reaction between **12** and 2 equiv of *p*-tolyl azide is *p*-tolyl-N=PPh_3 (identified by ^1H NMR and GC/MS), but it is unclear whether this product is formed by a nickel-mediated reaction that proceeds through an insipient "Ni^{III}=N-*p*-tolyl" fragment or by the direct reaction between dissociated PPh_3 and *p*-tolyl azide. The reaction between **13** and *p*-tolyl azide generates only a small amount of the carbodiimide *p*-tolyl-N=C=N^{t}Bu (^1H NMR, GC/MS).

We also surveyed the reaction between the Ni^I-L precursors and diazoalkanes as potential two-electron carbene transfer reagents. For example, we studied the reactivity of **14** and **15** in the presence of 2 equiv of Ph_2CN_2, Mes_2CN_2, ethyl diazoacetate, and trimethylsilyldiazomethane in benzene solution. Similar to the observations noted above, **14** is consumed more rapidly (hours) than **15** (days) at ambient temperature for each substrate except Mes_2CN_2, which does not react over a period of several days at room temperature. The resulting product mixtures invariably contain a variety of unidentified diamagnetic species. The absence of new paramagnetic species in the product profile suggests that terminal Ni^{III}=CR_2 species are not present.

Finally, we note that the reactivity of the Ni(0) species $\{[PhBP^{iPr}_3]NiL\}^-$ **20** and **21** to group transfer was also canvassed. These species were generated in situ by reduction of their Ni(I) precursors using sodium/mercury amalgam. Quantitative consumption of the Ni(I) species is confirmed by ^1H NMR spectroscopy, and subsequent addition of 2 equiv of an organic azide or diazoalkane leads in each case to rapid re-formation (<1 h) of the Ni(I) precursor (either **14** or **15**) in high yield. We suspect that the highly reducing $Ni(0)^-$ species are acting as electron-transfer reagents and affecting radical reduction of the organic substrate. A more systematic analysis of the organic products of these reactions was not undertaken.

IIg. Theoretical Considerations. We undertook the theoretical analysis of several hypothetical nickel complexes featuring a multiply bonded linkage to explore the feasibility of such species from an electronic structure perspective. To contextualize these results, it is instructive to first consider the L_2Ni=E fragments of Hillhouse and co-workers which are already known to give rise to isolable Ni=E complexes. Bonding considerations for these complexes have been addressed previously.[49] Figure 9A shows lobal representations of the frontier orbitals of an L_2M=E fragment as derived from the classic text of Albright, Burdett, and Whangbo.[50] The LUMO orbital is of b_2 symmetry (under C_{2v}) and is π^* in character. The much lower lying, filled M=E π-bonding orbital is not shown. As the transition is made from the L_2M=E fragment to the pseudotetrahedral L_3M-E structure under idealized 3-fold symmetry, the M−E linkage is more appropriately described as a bona fide triple bond (M≡E) for a d^6 configuration (Figure 9B).[14,49,51] For higher d-count configurations (d^7 or d^8) of similar geometry the formal bond order is lowered because the e-set is both σ^* (with respect to the phosphines) and π^* (with respect to the multiply bonded ligand) in character. The extent to which such configurations might be expected to be stable invariably depends on how energetically destabilized the upper π^* orbitals can lie while still housing an unpaired electron. The previously reported complexes $[PhBP_3]CoI$[14,52] and $[PhBP_3]Co(OSiPh_3)$[31] provide well-defined examples of pseudotetrahedral d^7 species with ^2E ground state configurations that serve as electronic models for the hypothetical $S = {}^1/_2$ $[BP_3]Ni^{III}(NR)$ systems under present consideration. An obvious issue concerns the extent to which the imide ligand, conventionally thought to be quite strongly π-donating, will

(49) (a) Albright, T. A.; Hoffmann, R.; Tse, Y.; D'Ottavio, T. *J. Am. Chem. Soc.* **1979**, *101*, 3812−3821. (b) Albright, T. A.; Hoffmann, R.; Thibeault, J. C.; Thorn, D. L. *J. Am. Chem. Soc.* **1979**, *101*, 3801−3812. (c) Glueck, D. S.; Wu, J.; Hollander, F. J.; Bergman, R. G. *J. Am. Chem. Soc.* **1991**, *113*, 2041−2054. (d) Cundari, T. R. *J. Am. Chem. Soc.* **1992**, *114*, 7879−7888.

(50) Adapted from: Albright, T. A.; Burdett, J. K.; Whangbo, M.-H. *Orbital Interactions in Chemistry;* Wiley & Sons: New York, 1985; pp 365, 383.

(51) Glueck, D. S.; Green, J. C.; Michelman, R. I.; Wright, I. N. *Organometallics* **1992**, *11*, 4221−4225.

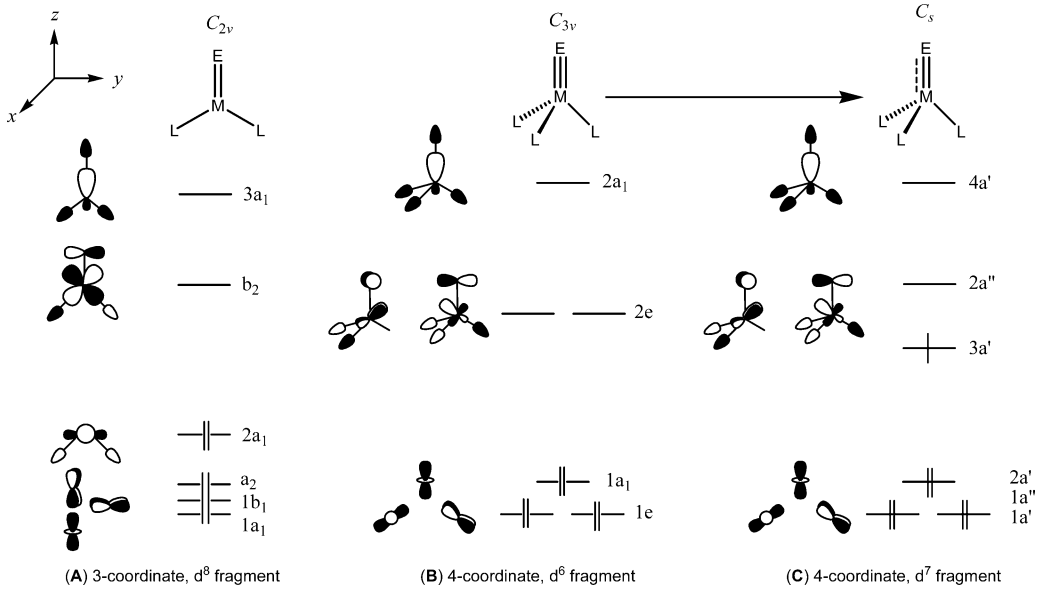

Figure 9. Qualitative molecular orbital diagrams for trigonal planar and pseudotetrahedral complexes containing Ni═E linkages. Idealized point groups and coordinate axes are indicated.

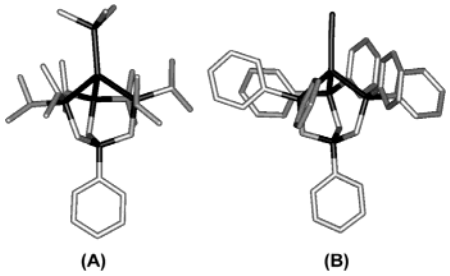

Figure 10. DFT optimized (Jaguar 5.0: B3LYP/LACVP**) molecular structures for (A) [PhBP$^{iPr}_3$]Ni(PMe$_3$) (optimized as a doublet ground state) and (B) [PhBP$_3$]Ni(NO) (optimized as a singlet ground state). Hydrogen atoms have been omitted for clarity.

destabilize such a system by raising the energy of the high-lying unpaired electrons for d^7 or d^8 configurations.

Figure 9B,C provides qualitative MO splitting diagrams that we can use to describe the electronic structure of putative d^6 L$_3$Ni^{IV}≡E and d^7 L$_3$Ni^{III}═E species. To examine the electronic structure of these structure types more thoroughly, we have calculated hypothetical structures (DFT) for a series of [PhBP$_3$] and [PhBP$^{iPr}_3$] nickel complexes. To establish a reasonable degree of confidence in the theoretical methods used, we first performed geometry optimizations for the synthetically isolable and structurally characterized complexes [PhBP$_3$]Ni(NO) (**16**) and [PhBP$^{iPr}_3$]Ni(PMe$_3$) (**14**). Using the Jaguar computational package (B3LYP/LACVP**), geometry optimizations were performed starting from the crystallographically determined coordinates of complexes **16** and **14** as the initial starting point in each case. As shown in Figure 10 and Table 1, the geometry optimized structures for **16** and **14** compare favorably with the experimentally determined solid-state structures. The most significant structural distinction worth noting is that the Ni−P bond distances are on average ∼0.1 Å longer in the DFT determined structures by comparison to the observed distances. As an additional check, the geometry of the optimized structure of [PhBP$_3$]Ni(NO) was evaluated for the correct number of imaginary frequencies through vibrational frequency calculations. No imaginary frequencies were located.

Table 1. Experimental and Calculated Bond Lengths and Angles for **14** and **16**

14	exptl	calcd	**16**	exptl	calcd
		Bond Lengths (Å)			
Ni−P4	2.263	2.358	Ni−N	1.624	1.665
Ni−P1	2.276	2.396	Ni−P1	2.232	2.309
Ni−P2	2.287	2.379	Ni−P2	2.215	2.316
Ni−P3	2.253	2.384	Ni−P3	2.234	2.315
		Angles (deg)			
P4−Ni−P1	121.90	122.45	N−Ni−P1	124.68	123.43
P4−Ni−P2	123.43	124.66	N−Ni−P2	119.84	125.67
P4−Ni−P3	118.67	117.44	N−Ni−P3	124.01	122.58
P1−Ni−P2	98.24	97.50	P1−Ni−P2	92.54	91.54
P1−Ni−P3	92.76	92.17	P1−Ni−P3	95.42	92.93
P2−Ni−P3	94.74	95.12	P2−Ni−P3	91.74	91.29
			Ni−N−O	176.0	177.9

We next examined the theoretical structures of several hypothetical Ni^{III} imides (Jaguar 5.0: B3LYP/LACVP**). As a starting point geometry for the theoretical optimization of $S = {}^1/_2$ [PhBP$_3$]Ni(N^{t}Bu), [PhBP$^{iPr}_3$]Ni(N^{t}Bu), and [PhBP$^{iPr}_3$]-Ni(NMe), we incorporated the *x*,*y*,*z* coordinates for the L$_3$-Ni−N framework from crystallographically determined coordinates for $S = 0$ [PhBP$^{iPr}_3$]Co≡NR and [PhBP$_3$]Co≡NR structures.[14,16] The DFT-minimized structure for [PhBP$_3$]-Ni(N^{t}Bu) is shown in Figure 11A. The complex features a rather short Ni−N bond distance (1.690 Å, Table 2) that is nonetheless appreciably longer (∼0.04 Å) than the Co−N and Fe−N bond distances observed for [PhBP$_3$]Co≡NR and [PhBP$_3$]Fe≡NR imide species, respectively.[14−16] This difference may be a manifestation of the attenuated Ni−N π-bond order in [PhBP$_3$]Ni(N^{t}Bu). Also of note from the structure is the significant variation in the three Ni−P bond distances. One Ni−P distance is significantly longer than the other two (2.429 Å vs 2.277 and 2.343 Å). The Ni−N−C imide angle is remarkably linear (179.28°). A similar overall geometry is obtained for the optimized structure of [PhBP$^{iPr}_3$]Ni(N^{t}Bu) (Figure 11B). In this latter structure,

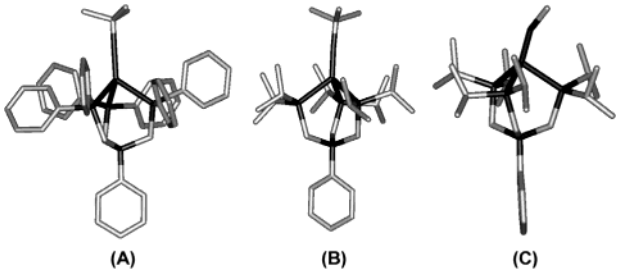

Figure 11. DFT optimized (Jaguar 5.0: B3LYP/LACVP**) molecular structures for (A) [PhBP$_3$]Ni(N^{t}Bu), (B) [PhBP$^{iPr}_3$]Ni(N^{t}Bu), and (C) [PhBP$^{iPr}_3$]Ni(NMe). Each geometry assumes a doublet ground state. Hydrogen atoms have been omitted for clarity.

Table 2. Bond Lengths and Angles of DFT Optimized Structures for [PhBP$_3$]Ni(N^{t}Bu), [PhBP$^{iPr}_3$]Ni(N^{t}Bu), and ([PhBP$^{iPr}_3$]Ni(NMe)

	[PhBP$_3$]Ni(N^{t}Bu)	[PhBP$^{iPr}_3$]Ni(N^{t}Bu)	[PhBP$^{iPr}_3$]Ni(NMe)
		Bond Lengths (Å)	
Ni−N	1.690	1.687	1.692
Ni−P1	2.429	2.519	2.378
Ni−P2	2.343	2.301	2.368
Ni−P3	2.277	2.303	2.320
		Angles (deg)	
Ni−N−C	179.28	176.90	156.99
P1−Ni−P2	89.85	90.70	94.93
P2−Ni−P3	88.81	92.25	91.90
P1−Ni−P3	89.45	90.78	91.26
N−Ni−P1	122.33	119.83	111.46
N−Ni−P2	126.35	124.54	114.04
N−Ni−P3	128.38	128.40	142.75

however, the elongated Ni−P bond distance is extremely elongated (2.519 Å). The elongation observed for one of the Ni−P bonds in [PhBP$^{iPr}_3$]Ni(N^{t}Bu) and [PhBP$_3$]Ni(N^{t}Bu) is fully consistent with the presence of a single electron in an orbital that is σ^* with respect to a N−P bond vector, as illustrated in Figure 9C. The distorted geometries we have previously reported for the structurally characterized low spin d^7 [PhBP$_3$]CoI and [PhBP$_3$]CoOSiPh$_3$ species provide experimental verification that this type of elongation is to be reasonably anticipated for such configurations.[25,31] That the DFT-minimized structure of [PhBP$^{iPr}_3$]Ni(N^{t}Bu) reveals such a pronounced distortion relative to [PhBP$_3$]Ni(N^{t}Bu) most likely reflects the respective σ donor character of the two borate auxiliaries. To probe whether steric factors might also be significantly contributing to the structure observed, the methyl imido complex [PhBP$^{iPr}_3$]Ni^{III}(NMe) was examined. As can be seen in Figure 11C, replacement of the *tert*-butyl group in [PhBP$^{iPr}_3$]Ni(N^{t}Bu) for a methyl group in [PhBP$^{iPr}_3$]-Ni(NMe) results in a dramatic distortion of the imido ligand. The Ni−N−C angle is now quite bent (156.99°). Moreover, in the [PhBP^{i}Pr$_3$]Ni(NMe) structure the three Ni−P bond distances show comparatively little variation. Thus, stabilization of the d^7 imide configuration is observed to occur by one of two processes. For a sterically encumbering imide, elongation of one Ni−P bond vector appears to be favored. For an imide that is less bulky, a severe bend in the imide functionality appears to be more energetically favorable such that a new geometry, better described as trigonal pyramidal with the imide ligand occupying an equatorial position, is obtained. Collectively, the DFT data obtained for these $S = {}^1/_2$ d^7 nickel imide species suggest that L$_3$Ni═NR may indeed be synthetically viable targets if (i) the L$_3$ ligand scaffold employed is sufficiently flexible to accommodate the anticipated distortion and (ii) bimolecular degradation pathways are not kinetically problematic.

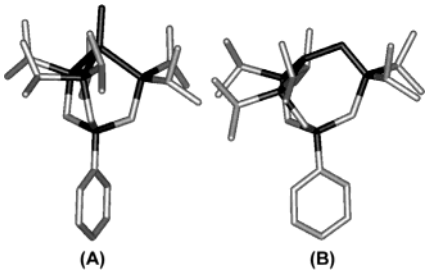

Figure 12. Starting point (A) and DFT optimized (Jaguar 5.0: B3LYP/LACVP**) geometry (B) for $S = 0$ [PhBP$^{iPr}_3$]Ni(N). Hydrogen atoms have been omitted for clarity.

The other structure type of interest to us concerns the hypothetical nickel nitride species [PhBP$^{iPr}_3$]Ni^{IV}≡N. As mentioned above, this d^6 species is formally isolobal and isoelectronic with the surprisingly stable d^6 cobalt imides that we have described previously.[14,16] However, there is an important distinction to be drawn between the relative d-orbital splitting energies between L$_3$M≡NR and L$_3$M≡N structure types due to the rehybridization at nitrogen that occurs. As we have recently suggested, the d orbital of a$_1$ symmetry in the d^4 complex [PhBP$^{iPr}_3$]Fe^{IV}≡N is highly destabilized due to a strong σ^* interaction between d$_{z^2}$ and the nitride σ donor.[18] The addition of two electrons to the frontier orbital diagram of [PhBP$^{iPr}_3$]Fe^{IV}≡N, which is provided by replacing the iron center by nickel, provides the electronic configuration (e)^4(a$_1$)^2(e)^0. Two electrons are therefore expected to lie at high energy for [PhBP$^{iPr}_3$]Ni^{IV}≡N, perhaps helping to explain why this species is not generated from [κ^2-PhBP$^{iPr}_3$]Ni(dbabh) (**11**) by loss of anthracene upon heating, whereas a similar synthetic strategy is quite effective for the case of iron. Thus, the electronic situation is quite distinct between a hypothetical [PhBP$^{iPr}_3$]Ni^{IV}≡N species and the known d^6 BP$_3$Co≡NR systems. In the latter species, the a$_1$ orbital of d$_{z^2}$ parentage is nearly degenerate with the nonbonding e-set.[14]

The consequences of electronic destabilization in [PhBP$^{iPr}_3$]-Ni≡N are manifest in its DFT-minimized structure. The starting and final geometries of this calculation are shown in Figure 12A,B. As can be seen, the nitride group inserts in a Ni−P bond in the optimized structure to afford a complex that is better viewed as a diamagnetic Ni(II) complex with one phosphinimato and two phosphine linkages. Whether this product is kinetically (or even thermodynamically) reasonable is unclear. In solution, bimolecular pathways to other structures, such as Ni$^{IV}_2$N$_2$ and Ni^{I}−N$_2$−Ni^{I}, might dominate. Regardless, the overall picture that begins to emerge is the following: for pseudotetrahedral structure types L$_3$Ni≡E, imide (NR^{2-}), and perhaps related carbyne (CR^{3-}) functionalities are more likely to electronically stabilize tetravalent nickel than terminal oxo or nitrido functionalities.

Conclusions

We have described synthetic entry to the chemistry of "[$PhBP_3$]Ni" and "[$PhBP^{iPr}_3$]Ni" systems. Most all of the complexes that have been prepared, for which the formal oxidation states Ni(0), Ni(I), and Ni(II) have been assigned, give rise to pseudotetrahedral geometries. For the divalent nickel complexes [$PhBP_3$]$Ni^{II}X$ in particular, small perturbations of the pseudotetrahedral geometry are observed that that depend on the nature of the X-type ligand employed. The unusual Ni(II) thiolate complex [$PhBP_3$]Ni(S-*p*-^{t}Bu-Ph) (**7**) is perhaps most distinct in this regard as it adopts a geometry that lies somewhere between that of a tetrahedron and a cis-divacant octahedron. The [$PhBP^{iPr}_3$]-containing Ni(II) complex [κ^2-$PhBP^{iPr}_3$]Ni(dbabh) (**11**) is in principle a precursor to a nickel(IV) nitride species but fails to evolve anthracene. Why this is the case is in part explained by theoretical considerations that suggest that a d^6 $L_3Ni{\equiv}N$ would feature a pair of electrons lying in a highly destabilized σ^* orbital. A general characteristic of the Ni(II) systems described is that access to pseudotetrahedral $L_3Ni^{II}X$ complexes where X represents a strong-field ligand, such as an alkyl or an amide, is problematic. This characteristic is also true of Riordan's tris(thioether)borate system [$PhTt^{tBu}$]$Ni^{II}X$.[38] When an amide can be installed, as for **11**, the structure type observed is three-coordinate trigonal planar. Electrochemical interrogation of the Ni(II) and Ni(I) complexes has revealed that reversible 1-electron $Ni^{II/I}$ and $Ni^{I/0}$ redox couples are accessible at fairly low potentials. Perhaps most striking is that the $Ni^{III/II}$ redox process is irreversible in all cases we have examined, even for ligands that are potentially good π-donors such as alkoxides and thiolates. This situation stands in contrast to related BP_3Fe and BP_3Co systems we have described, where the trivalent state is quite readily accessible. Whereas we had hoped that access to trivalent nickel might be possible by turning to dianionic imide and carbene functionalities in the fourth site ($L_3Ni^{III}{=}NR$ or $L_3Ni^{III}{=}CR_2$), the successful synthesis of such species has thus far eluded us. Simple MO considerations and DFT calculations nonetheless suggest that these types of complexes may be electronically accessible. We suspect that our inability to isolate well-defined examples of these types of species is due to synthetic nuances that we have yet to fully appreciate.

Experimental Section

All manipulations were carried out using standard Schlenk or glovebox techniques under a nitrogen atmosphere. Petroleum ether, benzene, toluene, diethyl ether, THF, dichloromethane, and acetonitrile were deoxygenated and dried by sparging with N_2 gas and passage through an activated alumina column. Hydrocarbon and ethereal solvents were tested with a standard purple solution of sodium benzophenone ketyl in tetrahydrofuran to ensure dioxygen and water removal. The compounds [$PhBP_3$]Tl,[52] [$PhBP^{iPr}_3$]Tl,[25b] Ph_2PCH_2Li(TMEDA),[53] $^iPr_2PCH_2Li$,[54] ASNBr,[55] Tl−O-*p*-^{t}Bu-Ph,[56] $TlOSiPh_3$,[57] KC_8,[58] Li−NH-2,6-^{i}Pr-Ph,[8] and lithium(dbabh)[41] were prepared according to literature methods. Deuterated solvents were purchased from Cambridge Isotopes Laboratories, Inc., and were degassed and stored over activated 3-Å molecular sieves prior to use. All other reagents and solvents were purchased from commercial vendors and used without further purification unless otherwise noted. ***CAUTION:*** *Thallium reagents are extremely toxic and should be handled and disposed of with care.*

Physical Methods. Elemental analyses were performed by Desert Analytics, Tucson, AZ. A Varian Mercury-300 spectrometer was used to record ^1H, $^{31}P\{^1H\}$, and $^{13}C\{^1H\}$ spectra at room temperature unless otherwise noted. ^1H and $^{13}C\{^1H\}$ chemical shifts were referenced to residual solvent. $^{31}P\{^1H\}$ NMR are reported relative to an external standard of 85% H_3PO_4 (0 ppm). Abbreviations for reported signal multiplicities are as follows: s, singlet; d, doublet; t, triplet; q, quartet; m, multiplet; br, broad. IR spectra were recorded on a Bio-Rad Excalibur FTS 3000 spectrometer controlled by Win-IR Pro software using a KBr solution cell. Solution magnetic moments were measured at 298 K in C_6D_6 following the Evans method.[59] MS data were obtained by injection of a hydrocarbon solution onto a Hewlett-Packard 1100MSD mass spectrometer (ES^+) or an Agilent 5973 mass selective detector (EI). UV−vis measurements were recorded on a Varian Cary 50 Bio Spectrophotometer controlled by Cary WinUV software. All measurements were recorded using a quartz cell fitted with a Teflon cap. X-ray diffraction studies (Table 3) were carried out in the Beckman Institute Crystallographic Facility on a Bruker Smart 1000 CCD diffractometer. Cyclic voltammetry measurements were recorded using a BAS CV 100W (Bioanalytical Systems Inc., West Lafayette, IN) using a glassy carbon working electrode, a platinum wire auxiliary electrode, and an $Ag/AgNO_3$ nonaqueous reference electrode filled with THF and Bu_4NPF_6. All electrochemical measurements are referenced to Fc/Fc^+ as an internal standard and can be corrected to SCE by adding 0.56 V to reported potential.[60]

Computational Methods. All calculations were performed using the hybrid DFT functional B3LYP as implemented in the Jaguar 5.0 program package.[61] This DFT functional utilizes the Becke three-parameter functional[62] (B3) combined with the correlation functional of Lee, Yang, and Parr[63] (LYP). The Ni was described using the LACVP basis set with the valence double-ζ contraction of the basis functions, LACVP**. All electrons were used for the other elements using Pople's[64] 6-31G** basis set. Input coordinates were derived as described in the text from crystallographically determined structures. Spin states and molecular charges were explicitly stated, and no molecular symmetry was imposed. Default values for geometry and SCF iteration cutoffs were used, and all

(52) Shapiro, I. R.; Jenkins, D. M.; Thomas, J. C.; Day, M. W.; Peters, J. C. *Chem. Commun.* **2001**, 2152−2153.

(53) (a) Peterson, D. J. *J. Organomet. Chem.* **1967**, *8*, 199−208. (b) Schore, N. E.; Benner, L. S.; Labelle, B. E. *Inorg. Chem.* **1981**, *20*, 3200−3208.

(54) Thomas, J. C.; Peters, J. C. *Inorg. Chem.* **2003**, *42*, 5055−5073.

(55) Blicke, F. F.; Hotelling, E. B. *J. Am. Chem. Soc.* **1954**, *76*, 5099−5103.

(56) Jazdzewski, B. A.; Holland, P. L.; Pink, M.; Young, V. G., Jr.; Spencer, D. J. E.; Tolman, W. B. *Inorg. Chem.* **2001**, *40*, 6097−6107.

(57) Harvey, S.; Lappert, M. F.; Raston, C. L.; Skelton, B. W.; Srivastava, G.; White, A. H. *J. Chem. Soc., Chem. Commun.* **1988**, *17*, 1216−1217.

(58) Schwindt, M.; Lejon, T.; Hegedus, L. *Organometallics* **1990**, *9*, 2814−2819.

(59) (a) Evans, D. F. *J. Chem. Soc.* **1959**, 2003−2005. (b) Sur, S. K. *J. Magn. Reson.* **1989**, *82*, 169−173.

(60) For information regarding correcting redox potenials vs Fc^+/Fc in various solvents see: Connelly, N. G.; Geiger, W. E. *Chem. Rev.* **1996**, *96*, 877−910.

(61) Jaguar 5.0, Schrodinger, LLC, Portland, Oregon, 2002.

(62) Becke, A. D. *J. Chem. Phys.* **1993**, *98*, 5648−5652.

(63) Lee, C.; Yang, W.; Parr, R. G. *Phys. Rev. B* **1988**, *37*, 785−789.

(64) (a) Hariharan, P. C.; Pople, J. A. *Chem. Phys. Lett.* **1972**, *16*, 217−219. (b) Francl, M. M.; Pietro, W. J.; Hehre, W. J.; Binkley, J. S. Gordon, M. S.; DeFrees, D. J.; Pople, J. A. *J. Chem. Phys.* **1982**, *77*, 3654−3665.

Table 3. X-ray Diffraction Experimental Details for **2**−**5**, **7**, **8A**,**B**, and **11**−**16**

	2	**3**	**4**	**5**	**7**
chem formula	$C_{45}H_{41}BINiP_3$·$0.5C_6H_6$	$C_{27}H_{53}BClNiP_3$	$0.84C_{45}H_{41}BN_3NiP_3$·$0.16C_{45}H_{41}BClNiP_3$	$C_{63}H_{56}BNiOP_3Si$·$1.5C_6H_6$	$C_{55}H_{54}BNiP_3S$
fw	871.14 + 39.05	575.57	821.69	1136.76	909.47
T (°C)	−177	−177	−177	−177	−177
λ (Å)	0.71073	0.71073	0.71073	0.71703	0.71703
a (Å)	22.502(3)	9.4015(8)	40.37(3)	13.1627(14)	38.222(2)
b (Å)	12.694(2)	11.5998(10)	12.887(15)	14.3575(15)	38.2222(2)
c (Å)	29.393(7)	29.392(3)	16.067(12)	17.2349(18)	12.5712(9)
α (deg)	90	90	90	101.988(2)	90
β (deg)	90.418(12)	90	111.48(6)	112.185(2)	90
γ (deg)	90	90	90	90.580(2)	90
V (Å^3)	8396(3)	3205.4(5)	7779(13)	2936.1(5)	18366.0(19)
space group	$P2_1/c$	$P2_12_12_1$	$C2/c$	$P\bar{1}$	I_1/a
Z	8	4	8	2	16
D_{calcd} (g/cm^3)	1.440	1.193	1.403	1.286	1.316
μ (cm^{-1})	13.45	8.52	7.29	4.78	6.10
R1, wR2[a] ($I > 2\sigma(I)$)	0.0494, 0.0824	0.0392, 0.0717	0.0489, 0.0708	0.0556, 0.0823	0.0523, 0.0649

	8A	**8B**	**11**	**12**
chem formula	$C_{45}H_{41}BClNiO_2P_3$·C_6H_6	$C_{90}H_{82}B_2Cl_2Ni_2O_4P_6$·$2C_7H_8$·$C_6H_6$·$CH_2Cl_{1.5}$	$C_{41}H_{63}BNNiP_3$	$C_{63}H_{56}BNiP_4$·$C_{9.95}$
fw	888.76	1952.89	732.35	1006.52 + 119.15
T (°C)	−177	−177	−177	−177
λ (Å)	0.71703	0.71703	0.71703	0.71073
a (Å)	16.2376(12)	24.8113(15)	12.0312(10)	19.9842(13)
b (Å)	16.4690(13)	13.9514(8)	26.359(2)	17.8132(11)
c (Å)	17.7364(14)	30.9581(19)	12.9206(11)	33.699(2)
α (deg)	90	90	90	90
β (deg)	113.379(1)	112.5030(10)	99.150(2)	90
γ (deg)	90	90	90	90
V (Å^3)	4353.6(6)	9900.3	4045.4(6)	11996.4(13)
space group	$P2_1/c$	$P2_1/n$	$P2_1/n$	$Pbca$
Z	4	4	4	8
D_{calcd} (g/cm^3)	1.356	1.310	1.202	1.247
μ (cm^{-1})	6.58	6.25	6.27	4.73
R1, wR2[a] ($I > 2\sigma(I)$)	0.0506, 0.0774	0.0697, 0.1129	0.0513, 0.0943	0.0573, 0.0951

	13	**14**	**15**	**16**
chem formula	$C_{50}H_{50}BNiP_3$	$0.95C_{30}H_{62}BNiP_4$·$0.05C_{27}H_{53}BP_3Tl$	$C_{32}H_{62}BNNiP_3$	$C_{45}H_{41}BNNiOP_3$
fw	827.34	619.37	623.26	774.22
T (°C)	−177	−177	−177	−177
λ (Å)	0.71703	0.71703	0.71703	0.71073
a (Å)	12.3572(10)	9.6258(5)	9.6300(7)	39.395(4)
b (Å)	13.6104(11)	21.6538(12)	12.2632(9)	12.9396(13)
c (Å)	15.1576(12)	16.8244(9)	15.4425(11)	16.1218(16)
α (deg)	75.775(1)	90	87.053(1)	90
β (deg)	70.824(1)	93.871(2)	80.119(1)	110.668(2)
γ (deg)	66.409(1)	90	84.968(1)	90
V (Å^3)	2187.3(3)	3498.8(3)	1788.5(2)	7682.2(13)
space group	$P\bar{1}$	$P2_1/c$	$P\bar{1}$	$C2/c$
Z	2	4	2	8
D_{calcd} (g/cm^3)	1.256	1.176	1.157	1.339
μ (cm^{-1})	5.88	9.35	6.97	6.67
R1, wR2[a] ($I > 2\sigma(I)$)	0.0411, 0.0669	0.0534, 0.0925	0.0410, 0.0876	0.0492, 0.0717

[a] $R1 = \sum||F_o| - \sum||F_c||/\sum|F_o|$, $wR2 = \{\sum|w(F_o^2 - F_c^2)^2|/\sum|w(F_o^2)^2|\}^{1/2}$.

structures converged under these criteria. The geometry of the optimized structure of [$PhBP_3$]Ni(NO) was evaluated for the correct number of imaginary frequencies through vibrational frequency calculations using the analytic Hessian. Zero imaginary frequencies correspond to a local minimum, whereas one imaginary frequency corresponds to a transition structure. No imaginary frequencies were found for [$PhBP_3$]Ni(NO). Further frequency calculations were precluded due to the impractical time requirements necessary to complete frequency calculations on molecules with so many non-hydrogen atoms.

Synthesis of [$PhBP_3$]NiCl (1). A benzene solution (30 mL) of [$PhBP_3$]Tl (0.313 g, 0.352 mmol) was added dropwise to a stirring suspension of $(Ph_3P)_2NiCl_2$ (0.230 g, 0.352 mmol) in benzene (10.0 mL). The reaction mixture was stirred at room temperature for 24 h and filtered through a Celite pad. The dark green filtrate was concentrated under reduced pressure to dryness to yield a dark green solid. The resulting solid was isolated on a medium porosity frit and washed three times with 4 mL portions of petroleum ether. The solid was then redissolved in benzene (10 mL) and filtered again through a Celite pad. Vapor diffusion of petroleum ether into the resulting green filtrate yielded analytically pure, green crystalline product (0.225 g, 82.0%). A second crop yielded an additional 0.192 g, 12%. ^{1}H NMR (300 MHz, C_6D_6): δ 26.1 (s), 8.3 (s), 7.6 (s), 7.5 (s), 1.22 (s), 0.89 (s), −6.8 (br s), −9.9 (s). UV−vis (C_6H_6)

λ_{max}, nm (ϵ): 434 (3332). μ_{eff} (C_6D_6, 298 K): 2.91 μ_B. Anal. Calcd for $C_{45}H_{41}BClNiP_3$: C, 69.32; H, 5.30. Found: C, 69.54; H, 5.69.

Synthesis of [$PhBP_3$]NiI (2). A benzene solution (30 mL) of [$PhBP_3$]Tl (0.561 g, 0.631 mmol) was added dropwise to a stirring suspension of NiI_2 (0.394 g, 1.26 mmol) in benzene (20 mL). The reaction mixture was stirred at room temperature for 24 h and filtered through a Celite pad. The resulting red-brown filtrate was concentrated under reduced pressure to 50% of original volume and filtered again through a Celite pad. Vapor diffusion of petroleum ether into the resulting red-brown filtrate produced brown, crystalline needles of the analytically pure product (0.472 g, 86%).^{1}H NMR (300 MHz, C_6D_6): δ 26.6 (s), 8.7 (s), 8.3 (s), 7.8 (s), 1.20 (s), 0.84 (s), −6.9 (br s), −11.07 (s). UV−vis (C_6H_6) λ_{max}, nm (ϵ): 705 (556), 446 (5612), 329 (7437). μ_{eff} (C_6D_6, 298 K): 2.87 μ_B. Anal. Calcd for $C_{45}H_{41}BINiP_3$: C, 62.04; H, 4.74. Found: C, 61.81; H, 4.93.

Synthesis of [$PhBP^{iPr}_3$]NiCl (3). In a 50 mL round-bottom flask, (DME)$NiCl_2$ (283.2 mg, 1.289 mmol) was suspended in THF (15 mL). A THF solution (20 mL) of [$PhBP^{iPr}_3$]Tl (882.0 mg, 1.286 mmol) was added dropwise over 10 min with vigorous stirring. After completion of the addition, the reaction mixture was stirred for 25 min and then filtered over Celite on a sintered glass frit. The solids and Celite were washed with benzene (10 mL). The combined filtrates were concentrated to dryness under reduced pressure. The resultant green-brown material was dissolved in benzene (10 mL) and filtered. Lyophilization of the filtrate provided green solid [$PhBP^{iPr}_3$]NiCl (716.8 mg, 96.8%). Crystals of **3** were grown from a concentrated solution in diethyl ether at −30 °C. ^{1}H NMR (300 MHz, C_6D_6): δ 37.1 (br s), 7.2−7.4 (m), 2.5 (br). μ_{eff} (C_6D_6, 298 K): 2.97 μ_B. UV−vis (C_6H_6) λ_{max}, nm (ϵ): 720 (330), 425 (3450), 385 (3340). Anal. Calcd for $C_{27}H_{53}BClNiP_3$: C, 56.34; H, 9.28. Found: C, 56.29; H, 8.92.

Synthesis of [$PhBP_3$]Ni(N_3) (4). A solution of **1** (0.171 g, 0.219 mmol) in THF (4 mL) was added to a stirring suspension of NaN_3 (1.43 g, 21.9 mmol) in THF (10 mL) at room temperature. After being stirred for 18 h, the yellow-green reaction mixture was filtered through a Celite pad and then evaporated to dryness under reduced pressure. The resulting solid was then extracted into benzene (3 mL) and filtered again through a Celite pad. Vapor diffusion of petroleum ether into the resulting yellow-green filtrate yielded yellow-green crystalline product (0.152 g, 88%).^{1}H NMR (300 MHz, C_6D_6): δ 25.4 (s), 8.02 (s), 7.5 (s), 7.4 (s), 1.25 (s), 0.47 (s), −6.6 (br s), −9.7 (s). UV−vis (C_6H_6) λ_{max}, nm (ϵ): 698 (310), 463 (3143), 328 (6285). μ_{eff} (C_6D_6, 298 K): 2.86 μ_B. IR: (C_6H_6) $\nu(N_3) = 2060$ cm^{-1}. Anal. Calcd for $C_{45}H_{41}BN_3NiP_3$: C, 68.74; H, 5.26; N, 5.34. Found: C, 68.37; H, 4.96; N, 4.93.

Synthesis of [$PhBP_3$]Ni($OSiPh_3$) (5). A solution of $TlOSiPh_3$ (0.0551 g, 0.115 mmol) in THF (2 mL) was added to a stirring solution of **1** (0.0897 g, 0.115 mmol) in benzene (4 mL). A white precipitate formed immediately. The reaction mixture was stirred for 2 h, filtered through a Celite pad, and evaporated to dryness under reduced pressure to yield a green solid. The green solid was extracted with benzene (2 mL) and filtered through a Celite pad. Vapor diffusion of petroleum ether into the filtrate provided bright green crystals of the analytically pure product (0.0984 g, 77%). ^{1}H NMR (300 MHz, C_6D_6): δ 24.3 (s), 8.7 (s), 7.4 (s), 6.9 (s), 1.39 (s), 0.92 (s), −4.6 (br s), −8.3 (s). UV−vis (C_6H_6) λ_{max}, nm (ϵ): 693 (353), 404 (3546). μ_{eff} (C_6D_6, 298 K): 2.95 μ_B. Anal. Calcd for $C_{70}H_{64}BNiOP_3Si$: C, 75.62; H, 5.80. Found: C, 76.02; H, 5.60.

Synthesis of [$PhBP_3$]Ni(O-*p*-^{t}Bu-Ph) (6). A solution of Tl(O-4-^{t}Bu-Ph) (0.0794 g, 0.225 mmol) in THF (4 mL) was added dropwise to a stirring solution of **1** (0.175 g, 0.225 mmol) in THF (5 mL). The reaction mixture was stirred for 3 h and concentrated to dryness under reduced pressure to yield a bright purple solid. The solid was extracted with benzene (3 mL) and filtered through a Celite pad. Vapor diffusion of petroleum ether into the benzene solution afforded the product as purple crystals (0.152 g, 76%). ^{1}H NMR (300 MHz, C_6D_6): δ 43.1 (br s), 23.9 (s), 4.3 (s), 3.6 (s), 2.7 (s), 0.3 (s), −4.3 (br s), −8.2 (s). UV−vis (C_6H_6) λ_{max}, nm (ϵ): 707 (1116), 524 (2437), 417 (3020). μ_{eff} (C_6D_6, 298 K): 2.87 μ_B. Anal. Calcd for $C_{55}H_{54}BNiOP_3$: C, 73.94; H, 6.09. Found: C, 73.67; H, 5.81.

Synthesis of Tl(S-*p*-^{t}Bu-Ph). 4-*tert*-Butylthiophenol (0.4418 g, 2.66 mmol) was dissolved in petroleum ether (10 mL). The colorless solution was then treated with Tl(OCH_2CH_3) (0.663 g, 2.66 mmol) as a petroleum ether solution (5 mL). The reaction mixture was stirred for 2 h, and the bright yellow solid that precipitated was collected on a medium porosity glass frit and washed with petroleum ether (15 mL) yielding yellow Tl(S-*p*-^{t}Bu-Ph) (0.812 g, 83%). Anal. Calcd for $C_{10}H_{13}STl$: C, 32.49; H, 3.54. Found: C, 32.58; H, 3.73.

Synthesis of [$PhBP_3$]Ni(S-*p*-^{t}Bu-Ph) (7). A solution of Tl(S-4-^{t}Bu-Ph) (0.0509 g, 0.138 mmol) in THF (3 mL) was added dropwise to a stirring solution of **1** (0.107 g, 0.138 mmol) in THF (4 mL). The reaction mixture was stirred for 3 h and concentrated to dryness under reduced pressure to yield a dark red solid. The solid was extracted with benzene (3 mL) and filtered through a Celite pad. Vapor diffusion of petroleum ether into the benzene solution yielded the product as red crystals (0.101 g, 81%). ^{1}H NMR (300 MHz, C_6D_6): δ 33.4 (br s), 22.8 (s), 8.6 (s), 2.8 (s), 2.7 (s), 0.3 (s), −4.9 (br s), −8.4 (s). UV−vis (C_6H_6) λ_{max}, nm (ϵ): 680 (778), 470 (3442). μ_{eff} (C_6D_6, 298 K): 3.02 μ_B. Anal. Calcd for $C_{55}H_{54}BNiOP_3$: C, 72.63; H, 5.98. Found: C, 72.54; H, 5.65.

Synthesis of [$PhB(CH_2P(O)Ph_2)_2(CH_2PPh_2)$]NiCl (8A). A solution of **1** (0.0850 g, 0.109 mmol) in benzene (4 mL) was treated with O_2 gas (8.0 mL, 0.327 mmol) with stirring at room temperature. The color of the reaction mixture changed from bright green to purple over the course of 6 h. Volatiles were removed under reduced pressure to yield a dark purple solid. This solid was extracted into toluene and filtered through a Celite pad. The filtrate was layered with petroleum ether and stored at −40 °C to afford the bright yellow crystalline product (0.0712 g, 80%).

{**[$PhB(CH_2P(O)Ph_2)_2(CH_2PPh_2)$]Ni($\mu$-Cl)**}$_2$ **(8B). 8B** was prepared as above with the following exception: The dark purple solid was extracted into benzene and filtered through a Celite pad. Slow diffusion of petroleum ether into the benzene solution at room temperature yielded the product as bright purple crystals (0.0782 mg, 94%).^{1}H NMR (300 MHz, C_6D_6): δ 19.2 (s), 9.6 (s), 8.4 (s), 8.1 (s), 7.8 (s), 5.8 (s), −0.68 (br s), −2.4 (s), −9.9 (s), −15.3 (s). UV−vis (C_6H_6) λ_{max}, nm (ϵ): 901 (323), 505 (634). Anal. Calcd for $C_{90}H_{82}Cl_2B_2Ni_2O_4P_6 \cdot 2C_7H_8 \cdot C_6H_6 \cdot CH_2Cl_{1.5}$: C, 68.67; H, 5.31. Found: C, 68.58; H, 5.15.

Synthesis of [$PhBP_3$]Ni(η^2-CH_2-PPh_2) (9). Method A. A 0.21% Na/Hg amalgam was prepared by dissolving metallic sodium (8.1 mg, 0.36 mmol) in mercury (3.70 g). A THF solution (10 mL) of **2** (0.307 g, 0.352 mmol) was added dropwise to a stirring suspension of the amalgam in THF (5 mL). The reaction mixture was stirred for 24 h, during which the color changed from red-brown to bright red. The THF solution was decanted away from the Hg and removed under reduced pressure to yield a bright red solid. This solid was extracted into toluene (3 mL) and filtered through a Celite pad. The resulting deep red filtrate was stored at −40 °C overnight and afforded red crystalline product (139 mg, 42%). **Method B.** A solution of **1** (0.114 g, 0.146 mmol) in toluene (4.0 mL) was cooled to −78 °C. A toluene solution (2 mL) of Ph_2PCH_2Li(TMEDA) (0.047 g, 0.146 mmol) was cooled to −78 °C and added dropwise to the solution of **1**. The reaction mixture was

allowed to warm to room temperature over a 6 h period, during which the color changed from dark green to blood red. The reaction mixture was filtered through a Celite pad, and the red filtrate was layered with petroleum ether and stored at −40 °C overnight to afford a red microcrystalline product. The product was isolated on a medium porosity frit and washed twice with 2 mL portions of diethyl ether (0.109 g, 80%). ^{1}H NMR (300 MHz, C_6D_6): δ 8.16 (d, 2H, J = 7.2 Hz), 7.66 (t, 2H, J = 7.2 Hz), 7.44 (m, 5H), 7.24 (m, 12H), 6.89 (m, 24H), 1.90 (br, 6H), 1.60 (q, 2H, J = 7.80 Hz). ^{13}C{^{1}H} NMR (75.4 MHz, C_6D_6): δ 167.1 (m), 141.3 (m), 133.4 (d, J_{P-C} = 12.1 Hz), 132.5 (m), 132.1(s), 129.8 (d, J_{P-C} = 3.5 Hz), 128.8 (s), 128.6 (s), 125.1(s), 30.1 (br), −9.5 (m). ^{31}P{^{1}H} NMR (121.4 MHz, C_6D_6): δ 22.28 (d, 3P, $^2J_{P-P}$ = 53 Hz), 29.20 (q, 1P, $^2J_{P-P}$ = 53 Hz). UV−vis (C_6H_6) λ_{max}, nm (ϵ): 544 (882), 435 (2670). Anal. Calcd for $C_{58}H_{53}BNiOP_4$: C, 73.84; H, 5.66;. Found: C, 73.49; H, 5.45.

Synthesis of [PhBP$^{iPr}_3$]Ni(η^2-CH$_2$P^{i}Pr$_2$) (10). A THF solution (2 mL) of ^{i}Pr$_2$PCH$_2$Li (23.3 mg, 0.169 mmol) was added dropwise to a stirring THF solution (2 mL) of **3** (95.9 mg, 0.167 mmol). The color of the reaction changed from pale green to yellow. After 30 min, volatiles were removed under reduced pressure. The solids were extracted with benzene (1 mL) and filtered. Volatiles were removed under reduced pressure, providing yellow **10** (103.1 mg, 92.0%). Attempts to obtain satisfactory elemental analysis for this compound have not been successful thus far. ^{1}H NMR (300 MHz, C_6D_6): δ 8.01 (br d, 2H, $^3J_{H-H}$ = 6.6 Hz), 7.49 (t, 2H, $^3J_{H-H}$ = 7.5 Hz), 7.26 (t, 1H, $^3J_{H-H}$ = 7.5 Hz), 1.84 (br m, 6H), 1.13 (m, 36H), 0.75 (m, 12H), −0.28 (s, 2H). ^{13}C{^{1}H} NMR (75.4 MHz, C_6D_6): δ 165.6 (q, $^1J_{B-C}$ = 47 Hz), 132.93, 126.77, 123.39, 26.33 (br), 21.08, 20.85, 20.35 (d, J_{P-C} = 6.4 Hz), 19.87 (d, J_{P-C} = 5.1 Hz), 19.71, 19.51 (d, J_{P-C} = 7.4 Hz), −12.84 (doublet of quartets, $^1J_{P-C}$ = 15.9 Hz, $^2J_{P-C}$ = 5.8 Hz). ^{31}P{^{1}H} NMR (121.4 MHz, C_6D_6): δ 49 (br, 3P), −18.2 (q, 1P, $^1J_{P-P}$ = 41 Hz). ^{11}B{^{1}H} NMR (128.3 MHz, C_6D_6): δ −15.7.

Synthesis of [κ^2-PhBP$^{iPr}_3$]Ni(dbabh) (11). A diethyl ether suspension (2 mL) of Hdbabh[41] (11.4 mg, 59.0 μmol) was frozen in a liquid nitrogen cooled well. To the stirring, thawing suspension was added a hexanes solution of *n*-butyllithium (1.6 M, 40 μL, 64 μmol). The reaction mixture was stirred and warmed at room temperature for 30 min. The resulting solution and a diethyl ether solution of **3** (33.9 mg, 58.9 μmol) were frozen in a liquid nitrogen cooled well. The two solutions were thawed, and the thawing solution of **3** was added to the thawing solution of [Li][dbabh]. The yellow-green reaction mixture was stirred and warmed. As the mixture warmed, a color change to inky green brown occurred. After 45 min of warming, the volatiles were removed under reduced pressure. The dark solids were extracted with petroleum ether (3 mL) and filtered. Crystals were obtained from the petroleum ether solution by cooling to −30 °C for several days. The crystals were analyzed as **11** (26.4 mg, 61.3%). ^{1}H NMR (300 MHz, C_6D_6): δ 7.75 (d, 2H, $^3J_{H-H}$ = 7.5 Hz), 7.41 (t, 2H, $^3J_{H-H}$ = 7.5 Hz), 7.21 (t, 1H, $^3J_{H-H}$ = 7.2 Hz), 6.98 (dd, 4H, J_{H-H} = 1.8, 2.7 Hz), 6.72 (dd, 4H, J_{H-H} = 1.8, 3.0 Hz), 5.44 (s), 1.57 (septet, 6H, J = 7.5 Hz), 1.18 (d, 18H, J = 7.3 Hz), 1.1 (br m), 0.82 (d, 18H, J = 7.5 Hz). ^{31}P{^{1}H} NMR (121.4 MHz, C_6D_6): δ 58 (br). Anal. Calcd for $C_{41}H_{63}BNNiP_3$: C, 67.24; H, 8.67; N, 1.91. Found: C, 67.18; H, 8.83; N, 1.48.

Synthesis of [PhBP$_3$]Ni(PPh$_3$) (12). Solid PPh_3 (0.191 g, 0.727 mmol) was added to a stirring solution of **1** (0.567 g, 0.727 mmol) in THF (7 mL). A THF solution (3 mL) of KC_8 (0.108 g, 0.799 mmol) was added to the reaction mixture and stirred for 12 h. Over this time period the color changed from bright green to bright yellow. All volatiles were removed under reduced pressure to yield a yellow solid. This solid was extracted into benzene and filtered through a Celite pad. Slow diffusion of petroleum ether into the yellow filtrate produced yellow crystals of the product (0.711 g, 95%). ^{1}H NMR (300 MHz, C_6D_6): δ 42.3 (s), 26.1 (s), 11.7 (s), 9.1 (s), 8.6 (s), 8.0 (s), 7.7 (br s), 6.3 (br), 5.1 (s), 0.60 (br), 0.30 (s), −9.9 (s). μ_{eff} (C_6D_6, 298K): 1.91 μ_B. UV−vis (C_6H_6) λ_{max}, nm (ϵ): 443 (1927). Anal. Calcd for $C_{64}H_{58}NiP_4$: C, 75.32; H, 5.73. Found: C, 75.38; H, 5.91.

Synthesis of [PhBP$_3$]Ni(CN^{t}Bu) (13). A 0.23 wt % amalgam was prepared by dissolving sodium (2.7 mg, 0.118 mmol) in mercury (1.18 g). Liquid ^{t}BuNC (9.8 mg, 0.118 mmol) was added to a THF solution (3 mL) of **1** (0.0916 g, 0.118 mmol) to produce an immediate color change from dark green to purple. This solution was then added dropwise to the stirring amalgam, and the reaction mixture was stirred for 12 h. Over this time period the reaction mixture changed from purple to burgundy. The burgundy solution was decanted away from the amalgam and dried under reduced pressure to yield a solid. The solid was extracted into benzene and filtered through a pad of Celite. Vapor diffusion of petroleum ether into the filtrate yielded red block crystals of the product (0.0761 g, 78%). ^{1}H NMR (300 MHz, C_6D_6): δ 12.52 (s), 8.9 (s), 7.9 (s), 7.7 (s), 0.47 (s), −6.6 (br s), −9.7 (s). UV−vis (C_6H_6) λ_{max}, nm (ϵ): 1059 (224), 443 (1409), 342 (8580). μ_{eff} (C_6D_6, 298 K): 1.74 μ_B. IR (C_6H_6, KBr), cm^{-1}, ν(CN): 2094. Anal. Calcd for $C_{50}H_{50}BNNiP_3$: C, 72.58; H, 6.09; N, 1.69. Found: C, 72.29; H, 6.07; N, 1.30.

Synthesis of [PhBP$^{iPr}_3$]Ni(PMe$_3$) (14). In a 20 mL vial, [PhB(CH$_2$P^{i}Pr$_2$)$_3$]NiCl (227.7 mg, 395.6 μmol) was dissolved in THF (8 mL). Neat PMe_3 (614 μL, 5.93 mmol) was added to the solution, causing the reaction mixture to become dark red. After 10 min, the homogeneous reaction mixture was transferred to a vial containing a stirbar and sodium/mercury amalgam (0.378% w/w, 2.4022 g, 395 μmol of sodium atoms). The reaction mixture was stirred vigorously for 4 h, during which time the color became yellow-orange. The reaction mixture was filtered over Celite on glass fiber filter paper, and the Celite was washed with benzene [3 × 2 mL]. The combined filtrates were concentrated to dryness under reduced pressure, providing analytically pure yellow-orange solid **14** (239.4 mg, 98.4%). Crystals of **14** were grown from a diethyl ether/petroleum ether mixture at −30 °C. ^{1}H NMR (300 MHz, C_6D_6): δ 35.3 (br s, 6H), 16.5 (br s, 9H), 11.0 (br s, 6H), 10.1 (br s, 18H), 9.0 (s, 2H), 8.0 (t, 2H, J = 7.2 Hz), 7.7 (t, 1H, J = 7.5 Hz), −0.3 (br s, 18H). μ_{eff} (C_6D_6, 298 K): 1.82 μ_B. UV−vis (C_6H_6) λ_{max}, nm (ϵ): 430 (1240). Anal. Calcd for $C_{30}H_{62}BNiP_4$: C, 58.47; H, 10.14. Found: C, 58.50; H, 10.30.

Alternative Synthesis. Solid yellow $(COD)_2Ni$ (49.5 mg, 180 μmol) was dissolved in petroleum ether (3 mL). Neat PMe_3 (75 μL, 725 μmol) was added with stirring. After 1 h, a benzene solution (3 mL) of [PhBP$^{iPr}_3$]Tl (123.5 mg, 180.1 μmol) was added to the pale yellow reaction mixture. Upon addition, the reaction mixture darkened. Over 48 h, gray solids precipitated from solution. Volatiles were removed from the reaction mixture under reduced pressure. The solids were extracted with petroleum ether (10 mL) and filtered. Crystallization of the petroleum ether solution at −30 °C over 3 days provided yellow crystals of **14**. Analysis of the crystals by ^{1}H NMR and ^{31}P{^{1}H} NMR spectroscopy showed the presence of [PhB(CH$_2$P^{i}Pr$_2$)$_3$]Ni(PMe$_3$) and [PhB(CH$_2$P^{i}Pr$_2$)$_3$]Tl, in a 95:5 ratio. ^{1}H NMR (300 MHz, C_6D_6): δ 35.3 (br s, 6H), 16.5 (br s, 9H), 11.0 (br s, 6H), 10.1 (br s, 18H), 9.0 (s, 2H), 8.0 (t, 2H, J = 7.2 Hz), 7.7 (t, 1H, J = 7.5 Hz), 7.1−7.3 (m, [PhB(CH$_2$P^{i}Pr$_2$)$_3$]Tl), 1.90 (br, [PhB(CH$_2$P^{i}Pr$_2$)$_3$]Tl), 1.21 (br, [PhB(CH$_2$P^{i}Pr$_2$)$_3$]Tl), 1.07 (m, [PhB(CH$_2$P^{i}Pr$_2$)$_3$]Tl), −0.3 (br s, 18H). ^{31}P{^{1}H} NMR (121.4 MHz, C_6D_6): δ 45.35 (d, $^1J_{Tl-P}$ = 5910 Hz).

Synthesis of [PhBP$^{iPr}_3$]Ni(CN^{t}Bu) (15). To a benzene solution (3 mL) of **14** (91.3 mg, 148 μmol) was added dropwise a benzene solution (2 mL) of CN^{t}Bu (67.7 mg, 814 μmol). The reaction mixture darkened to orange-red. The reaction mixture was stirred for 20 min. The solution was filtered and concentrated to dryness under reduced pressure. The resulting orange-red material was dissolved in toluene (1 mL), and concentrated to dryness under reduced pressure. The toluene evaporation procedure was repeated twice more, providing yellow-orange solid **15** (78.7 mg, 85.4%). Crystals of **15** were grown from a diethyl ether/petroleum ether solution at −30 °C. ^{1}H NMR (300 MHz, C_6D_6): δ 47.9 (br s, 6H), 12.6 (br s, 6H), 11.3 (br s, 18H), 8.8 (s, 2H), 7.8 (s, 2H), 7.6 (t, 1H, J = 7.5 Hz), 3.0 (s, 9H), 0.3 (br s, 18H). μ_{eff} (C_6D_6, 298 K): 1.68 μ_B. UV−vis (C_6H_6) λ_{max}, nm (ϵ): 430 (1560). IR (THF, KBr) cm^{-1}, ν(CN): 2056. Anal. Calcd for $C_{32}H_{62}BNNiP_3$: C, 61.67; H, 10.03; N, 2.25. Found: C, 61.39; H, 10.35; N, 2.00.

Alternative Synthesis. Solid green **3** (81.0 mg, 141 μmol) was dissolved in THF (3 mL). Neat CN^{t}Bu (40 μL, 660 μmol) was added and the reaction mixture was stirred, forming a golden orange solution. After 20 min, the ^{31}P{^{1}H} NMR spectrum was examined. ^{31}P{^{1}H} NMR (121.4 MHz, THF): δ 62.7 (br d), 47.7 (br d), 3.2 (br s). Volatiles were removed under reduced pressure. The resultant solids were dissolved in THF (2 mL) and added to a sodium/mercury amalgam (0.378% w/w, 859.0 mg, 141.2 μmol of sodium atoms), followed by washing with additional THF (3 mL). The reaction mixture was stirred vigorously for 3 h. The reaction mixture was filtered, providing an orange-yellow solution. Volatiles were removed under reduced pressure. The resultant solids were washed with petroleum ether [3 × 0.5 mL], removing an orange-red supernatant and leaving yellow solids. The solids were dried under reduced pressure, providing **15** (51.3 mg, 58.4%).

Synthesis of [PhBP$_3$]Ni(NO) (16). Method A. A solution of **12** (0.645 g, 0.641 mmol) in benzene (15 mL) was stirred under 1 atm of NO gas for 2 h. The color of the reaction mixture changed from bright yellow to dark red over this time period. The reaction mixture was concentrated to dryness under reduced pressure to yield a red solid. This solid was extracted into benzene (4 mL) and filtered through a Celite pad. Vapor diffusion of petroleum ether into the red filtrate yielded red crystalline product (0.452 g, 91%). **Method B.** A solution of **1** (0.215 g, 0.276 mmol) in benzene (4 mL) was treated with NO gas (13.6 mL, 0.552 mmol) and stirred for 2 h. Over this time period the reaction mixture changed from dark green to dark red. The solution was concentrated under reduced pressure to 50% of its original volume and filtered through a Celite pad. Vapor diffusion of petroleum ether into the red filtrate yielded crystalline dark red product (0.193 g, 90%). ^{1}H NMR (300 MHz, C_6D_6): δ 8.01 (d, 2H, J = 6.6 Hz), 7.76 (m, 7H), 7.55 (m, 12H), 7.02 (t, 6H, J = 7.2 Hz), 6.78 (d, 15H, J = 6.6 Hz), 1.50 (br, 6H). ^{13}C NMR (C_6D_6, 75.4 MHz, 25 °C): δ 138.3 (m), 132.2−131.0 (overlapping resonances), 131.8 (dd, J = 4.3, 7.8 Hz) 131.4 (s), 129.5 (s), 129.3 (s), 128.3 (s), 124.9(s), 18.3 (br). ^{31}P{^{1}H} NMR (121.4 MHz, C_6D_6): δ 37.3. UV−vis (C_6H_6) λ_{max}, nm (ϵ): 913 (159), 433 (2206), 350 (2059). μ_{eff} (C_6D_6, 298K): 2.86 μ_B. IR (C_6H_6, KBr), cm^{-1}, ν(NO): 1737. Anal. Calcd for $C_{45}H_{41}BNNiOP_3$: C, 69.81; H, 5.34; N, 1.81. Found: C, 70.21; H, 5.18; N, 1.53.

Synthesis of [κ^2-PhBP$_3$]Ni(CO)$_2$][^{n}Bu$_4$N] (17). A benzene solution (3 mL) of [PhBP$_3$]Tl (0.276 g, 0.313 mmol) was added dropwise to a stirring benzene solution (3 mL) of $(PPh_3)_2Ni(CO)_2$ (0.200 g, 0.313 mmol). After stirring for 1 h, a THF solution (3 mL) of [^{n}Bu$_4$N][Br] (0.101 g, 0.313 mmol) was added to the reaction mixture and a white precipitate formed immediately. The reaction mixture was stirred for 12 h and was filtered through a Celite pad. All volatiles were removed under reduced pressure to yield a pale yellow solid. The solid was isolated on a medium porosity frit and washed twice with 2 mL portions of EtOH. Dissolving the solid in THF and layering with diethyl ether afforded crystalline product (0.272 g, 83%). ^{1}H NMR (300 MHz, C_6D_6): δ 8.15 (t, 2H, J = 8.0 Hz), 8.0 (m, 4H), 7.69 (d, 2H, J = 6.3 Hz), 7.55 (m, 6H), 7.27 (t, 2H, J = 6.0 Hz), 7.06 (m, 17H), 2.79 (br, 8H, [^{n}Bu$_4$N]), 2.61 (br, 6H), 1.16 (br, 16H, [^{n}Bu$_4$N]), 0.882 (br, 12H, [^{n}Bu$_4$N]). ^{13}C{^{1}H} NMR (75.4 MHz, acetone-d_6): δ 206.2 (t, J_{P-C} = 2.1 Hz), 149.0 (m), 138.6 (m), 134.5 (s), 134.3 (s), 134.0 (d, J = 4.5 Hz), 133.5 (s), 132.8 (s), 132.6 (s), 130.1 (s), 129.8 (s), 129.1 (d, J = 3.7 Hz), 129.0 (s), 128.2−127.1 (overlapping resonances), 126.6 (s), 59.5 (t, J_{C-N} = 2.9 Hz), 24.6 (s), 20.5 (s), 15.7 (br), 13.5 (s). ^{31}P{^{1}H} NMR (121.4 MHz, C_6D_6): δ 29.2 (s), −9.46 (br). IR (THF, KBr), cm^{-1}, ν(CO): 1994, 1913. Anal. Calcd for $C_{63}H_{77}BNNiO_2P_3$: C, 72.57; H, 7.44; N, 1.34. Found: C, 72.21; H, 7.06; N, 1.47.

Synthesis of [[κ^2-PhBP$^{iPr}_3$]Ni(CO)$_2$][ASN] (18). Solid [PhBP$^{iPr}_3$]Tl (317.1 mg, 0.4625 mmol), $(Ph_3P)_2Ni(CO)_2$ (296.2 mg, 0.4633 mmol), and ASNBr (96.1 mg, 0.466 mmol) were combined in THF (7 mL) and stirred in the dark. Monitoring of the reaction mixture by ^{31}P{^{1}H} NMR showed that all of the [PhBP$^{iPr}_3$]Tl had been consumed after 4 days. Volatiles were removed under reduced pressure, and benzene (1 mL) was added to the resulting sticky solids. A yellow oil separated, and the benzene was decanted. This procedure was repeated three times, the yellow oil being isolated each time. The yellow oil was placed under reduced pressure for several hours, providing sticky yellow solids. The solids were taken up in a mixture of THF and diethyl ether (2:1), and stored at −30 °C for 24 h. A small amount of white precipitate formed, which was removed by filtration. This precipitation process was repeated again. The resulting solution was concentrated to dryness under reduced pressure, to provide sticky yellow solids whose spectroscopic properties were consistent with **18** (129.3 mg, 38.7%). ^{1}H NMR (300 MHz, THF-d_8): δ 7.44 (br s, 2H), 6.87 (t, 2H, J = 7.5 Hz), 6.67 (t, 1H, J = 7.5 Hz), 3.49 (m, 8H), 2.19 (m, 8H), 1.91 (septet, 2H, J = 7.2 Hz), 1.64 (m, 4H), 1.18 (dd, 12H, J = 6.5, 7.2 Hz), 1.08 (m, 4H), 0.97 (m, 12H), 0.77 (dd, 12H, J = 6.2, 7.5 Hz), 0.28 (br, 2H). ^{13}C{^{1}H} NMR (75.4 MHz, THF-d_8): δ 208.16 (t, $^2J_{P-C}$ = 1.6 Hz), 169.08 (q, $^1J_{B-C}$ = 50 Hz), 133.66, 126.11, 122.20, 63.86 (t, $^1J_{N-C}$ = 3.2 Hz), 28.23, 27.30, 24.92 (d), 23.03, 21.23 (d), 20.71 (d), 20.45 (d), 20.10 (br), 19.81 (br), 19.73 (d). ^{31}P{^{1}H} NMR (121.4 MHz, THF-d_8): δ 51.13 (s, 2P), 4.80 (s, 1P). ^{11}B-{^{1}H} NMR (128.3 MHz, THF-d_8): δ −15.0. IR (THF, KBr) cm^{-1}, ν(CO): 2004, 1878.

Photolysis of [κ^2-PhBP$_3$]Ni(CO)$_2$][^{n}Bu$_4$N]. A THF (10 mL) solution of **17** (0.1274 g, 0.122 mmol) was transferred to a photolysis cell equipped with an N_2 inlet line and a gas outlet line connected to a mineral oil bubbler. The solution was photolyzed with a mercury lamp for 8 h. The solution was evaporated to dryness to yield a pale yellow solid. This solid was extracted into benzene solution and filtered through a Celite pad. Attempts to crystallize by slow evaporation of a benzene solution or slow diffusion of petroleum ether into a THF solution both yielded a yellow oil containing {[PhBP$_3$]Ni(CO)}{^{n}Bu$_4$N} (**22**) and a paramagnetic impurity. ^{1}H NMR (300 MHz, C_6D_6): δ 8.28 (t, J = 8.15 Hz, 2H), 8.03 (m, 6H), 7.63 (m, 6H), 7.49 (m, 1H), 7.06 (m, 9H), 6.75 (m, 13H) (br, 8H, [^{n}Bu$_4$N]), 1.49 (br, 6H), 1.16 (br, 16H, [^{n}Bu$_4$N]), 0.882 (b, 12H, [^{n}Bu$_4$N]). ^{31}P{^{1}H} NMR (121.4 MHz, C_6D_6): δ 25.33. IR: (THF, KBr) cm^{-1}, ν(CO): 1869.

Reactivity of 1 with Methyllithium. A diethyl ether (6 mL) solution of **1** (0.0831 g, 0.106 mmol) was cooled to −78 °C. A solution of methyllithium (1.6 M in hexanes, 1.71 mL, 0.106 mmol)

was added dropwise to this solution. The solution was warmed slowly to room temperature over the course of 4 h. During this time the color of the reaction mixture went from dark green to blood red. The solution was filtered through a pad of Celite to remove insoluble material. All volatiles were remove under reduced pressure to yield a dark-red solid. When extracted into benzene and analyzed by ^{1}H and $^{31}P\{^{1}H\}$ NMR, the reaction mixture exhibited the diamagnetic resonances of complex **9**.

Reactivity of 1 with Lithium Amides. A procedure similar to that reported for the reactions of **1** with methyllithium was followed. In all procedures, the lithium amides were added cold (−78 °C) to **1**. The solutions became dark red upon warming to room temperature. The products exhibited the same spectral signatures as complex **9**.

Reaction of 1 with $CoCp_2$. A THF (5 mL) solution of $CoCp_2$ (5 mL) was added dropwise to a (THF) solution of **1** (0.1889 g, 0.242 mmol). The reaction mixture was stirred for 1.5 h. [$^{n}Bu_4N$][Br] (0.0939 g, 0.242 mmol) was then introduced as a THF solution (3 mL), and the reaction mixture was stirred for an additional hour. The THF solution was filtered through a Celite pad to remove insoluble material, and the resulting red-brown solution was concentrated to dryness. The red-brown solid was collected on a medium porosity frit and washed with Et_2O. Crude ^{1}H NMR (300 MHz, C_6D_6): δ 21.5 (br), 12.2 (m), 11.8 (m), 8.4 (m), −3.6 (br) −5.8 (br), −47.6 (br). Attempts to recrystallize this product led to a mixture of diamagnetic and paramagnetic products.

Reaction of 12 with *p*-Tolyl Azide. Complex **12** (0.1103 g, 0.110 mmol) was dissolved in benzene. To this reaction mixture was added *p*-tolyl azide (29.3 mg, 0.22 mmol) drowise as a benzene solution (2 mL). After 15 min, the color changed from bright yellow to dark brown. The reaction mixture was stirred for 24 h, and all solvent was removed under reduced pressure. The only identifiable product in this reaction was *p*-tolyl-N═PPh_3. ^{1}H NMR (300 MHz, C_6D_6): δ 7.81 (m, 4H), 7.04 (m, 15H), 2.20 (s, 3H). $^{31}P\{^{1}H\}$ NMR (121.4 MHz, C_6D_6): δ −1.17 (s). ESI/MS (*m*/*z*): 368.1 (*p*-tolyl-N═PPh_3 + H^+).

Acknowledgment. We acknowledge the DOE (PECASE) and the NSF (CHE-0132216) for financial support of this work. Larry Henling, Smith Nielsen, and Eric Peters provided technical assistance. We are grateful to Professors Peter T. Wolczanski and Daniel Rabinovich for providing insightful discussions. We also thank Professor Clifford Kubiak for disclosing results prior to publication. The Beckman Institute Senior Research Fellows Program (CEM), the Moore Foundation (J.C.T.), the NSF (J.C.T.), and the DOD (T.A.B.) are each acknowledged for fellowship support.

Supporting Information Available: CIFs and tables of crystallographic data for complexes **2**−**5**, **7**, **8A**,**B**, and **11**−**16**, including fully labeled thermal ellipsoid plots, crystallographic details, atomic coordinates, equivalent isotropic displacement parameters, anisotropic displacement parameters, and interatomic distances and angles. This material is available free of charge via the Internet at http://pubs.acs.org.

IC049936P